MINISTERIO
DE ECONOMÍA
Y COMPETITIVIDAD

Instituto de Tecnologías
Físicas y de la Información

CSIC
CONSEJO SUPERIOR DE INVESTIGACIONES CIENTÍFICAS

TECHNICAL REPORT

Acoustic field in a cubic open cavity lined with MPPs

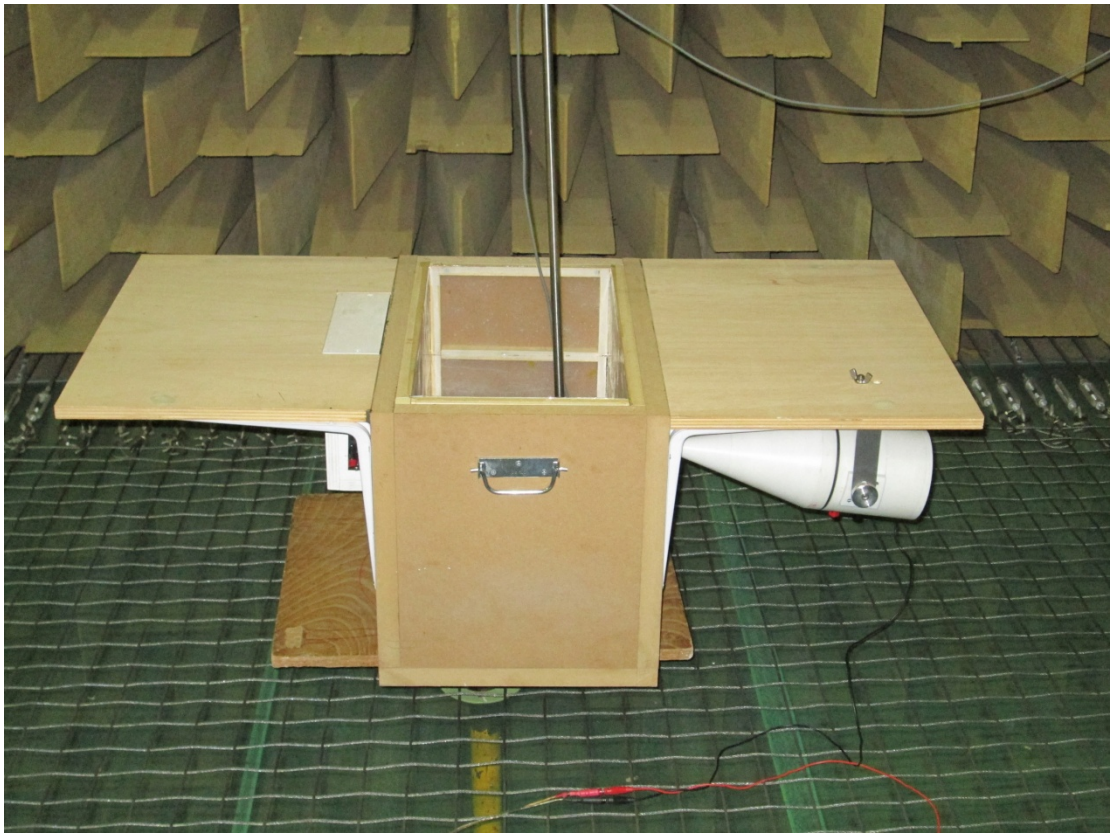

Santiago Ortiz, Cristobal González, Pedro Cobo

Environmental Acoustics Group, ITEFI, CSIC, Spain

January 2014

CONTENTS

1. INTRODUCTION

In a previous work, Ortiz *et al.* (2013) elucidated the acoustic resonances of a 3D open cavity by a fast and efficient method which models the time response at any point in the medium as the convolution of the source waveform with the impulse response of the cavity. Such impulse response was obtained as a sequence of attenuated and delayed impulses coming from the real and mirror imaged sources (Image Source Model, ISM). The transformation of the time response at any point to the frequency domain provided the Frequency Response Function (FRF) at such point. The peaks of the FRF were identified then as the resonance frequencies of the open cavity.

The proposed ISM method was experimentally validated on a 3D cubic open cavity made with medium density fibreboard panels of thickness 3 cm and dimensions (*W,L,D*)=(53,32,38) cm, Figure 1. A 4 " Sonavox Honeycom loudspeaker, located at the centre line of the front wall, was used as source. Since the peaks at the frequency response of the loudspeaker could be misinterpreted as resonances of the cavity, the loudspeaker was equalised by inverse filtering, as proposed by Cobo *et al.* (2007).

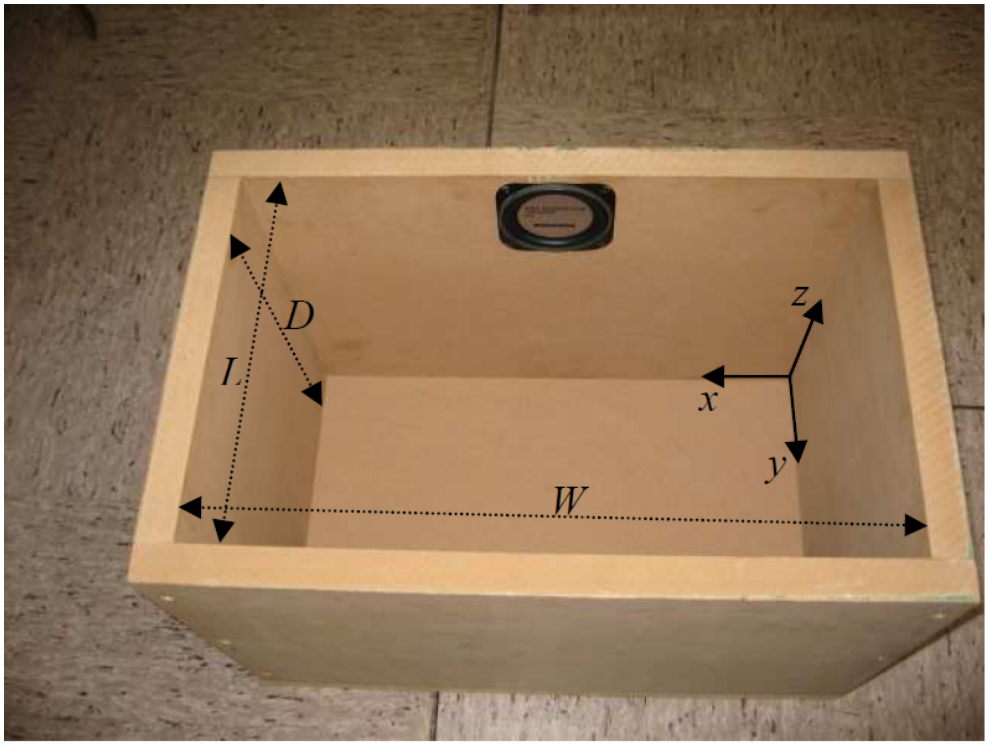

Figure 1. The 3D open cavity

The resonance frequencies obtained by the ISM method were compared with these measured experimentally. As shown in Table 1, the predicted resonances frequencies differ of these measured less than 4.5 %.

Table 1. Resonance frequencies of the open cavity (After Ortiz et al., 2013)

Peak at FRF	Mode (l, m, n)	f_{exp} (Hz)	f_{the} (Hz)	E (%)
1	(0,0,0)	157	151.4	3.6
2	(1,0,0)	374.5	Not seen	
3	(0,1,0)	575	549	4.5
4	(2,0,0)	680.9	659.8	3.1
5	(2,1,0)	863.4	854.5	1.0
6	(0,2,0)	1103	1090	1.2
7	(2,2,0)	1290	1270	1.6
8	(4,1,0)	1430	1431	0.1
9	(4,2,0)	1642	1646	0.2
10		1768	1763	0.3
11		2273	2255	0.8

Whereas the ISM model assumes a point source, the 4 " loudspeaker used cannot longer be considered a enough small source as compared with the dimensions of the cavity. Therefore, we decided to implement a better approach to a point source. Pollack *et al.* (2001) proposed a conventional loudspeaker feeding a small aperture through a reverse horn as an excellent approach to a point and omnidirectional source. This design was used successfully by Cobo *et al.* (2013) to construct an omnidirectional source for ground impedance measurements. However, this source is bulky and heavy, and it is hard to handle for measurements in the open cavity. Therefore, the same reverse horn design was used to build two new point sources, lighter and smaller than the source for ground impedance, and hence more appropriate for our current purpose (Ortiz *et al.*, 2014). Figure 2 shows such new point sources.

Whilst the reverse horn design is a good approach to a point source, its frequency response is rather irregular, due to the resonances of the air inside the horn. Fortunately, the inverse filtering is able to equalise also the frequency response of such source. Therefore, the inverse filtered reverse horn loudspeaker provides a point (omnidirectional) source with a flat frequency response in the range from 100 Hz to 8 kHz.

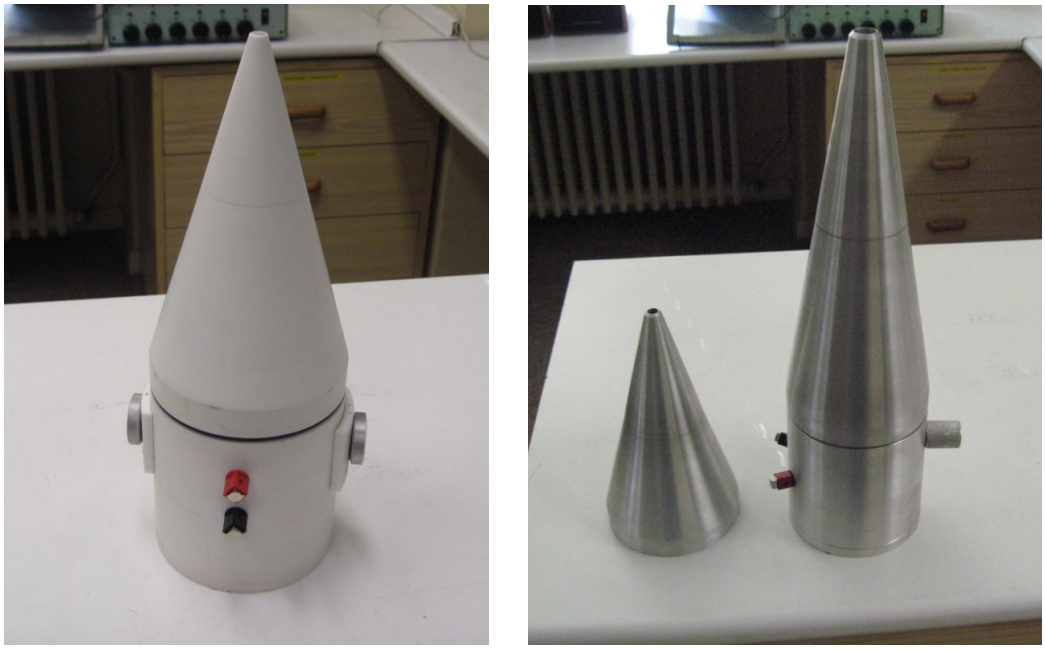

Figure 2. Two point sources for measurements in open cavities

The acoustic resonances in the open cavity can be decreased by noise control techniques. One passive control technique consists of lining the inner walls of the cavity with absorbing material. Whilst porous materials provide wideband absorption, they are discouraged in presence of air flow. Since open cavity tones are usually driven by air flow (wheel wells in airplanes, shallow cavity above bogies in trains, sunroof in cars), alternative absorbers supporting air flowing might be used. Microperforated panels (MPP) are recognised as the next generation absorbing materials. Furthermore, they can be used in presence of air flow (Cobo *et al.*, 2010). Their absorption curve can be reliably predicted by means of models which depend on the constitutive parameters of the MPP. Namely, its perforation diameter, d, thickness, t, perforation ratio, ϕ, and air cavity depth behind the panel, D.

The main shortcoming of constructing MPP absorbers, its high manufacturing cost, can be currently avoided by using the infiltration technique proposed by Cobo and Montero de Espinosa (2013). This technique consists of mixing common salt grains of controlled size and quantity with a commercial epoxy resin. When the mixture cures, the sample is introduced into a water tank to dissolve the salt grains, appearing the holes with the shape and size of the salt grains. Figure 3 shows an MPP manufactured by this technique.

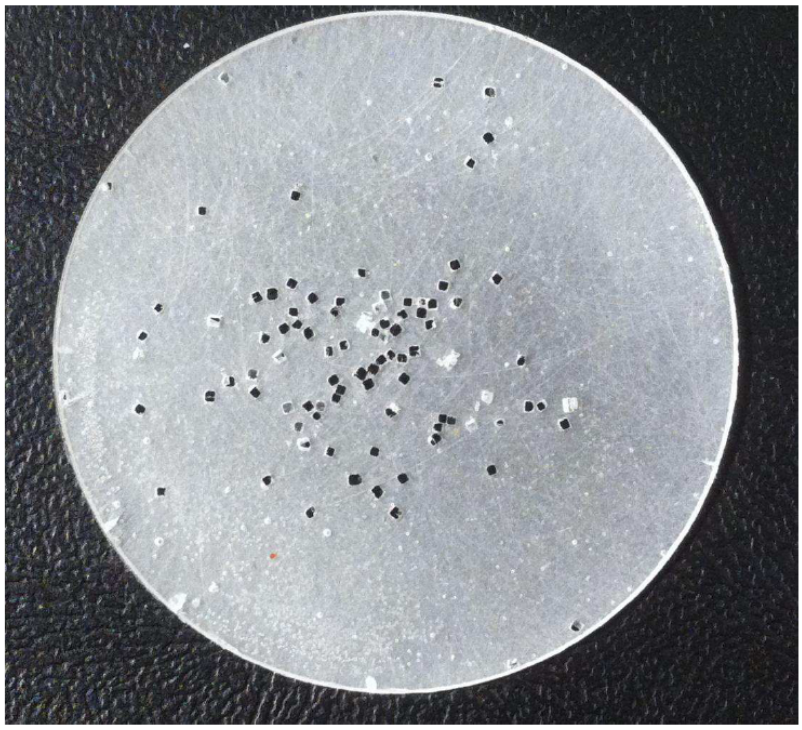

Figure 3. An MPP manufactured by infiltration (After Cobo and Montero de Espinosa, 2013)

The major aim of this work is to report the modification of the acoustic field in the open cavity shown in Figure 1 when its inner walls are lined with MPPs manufactured by infiltration similar to this shown in Figure 3, using one of the point sources shown in Figure 2. The open cavity will be described in Section 2. Section 3 will review the characteristics of the point source used for measuring the acoustic resonances of the cavity. The MPPs used to line the inner walls of the cavity will be analysed in Section 4. The measuring procedure and the experimental results will be explained in Sections 5 and 6, respectively. Finally, the main conclusions will be disclosed in Section 7.

2. THE CUBIC OPEN CAVITY

A cubic 3D open cavity was made with DM wood panels of thickness 3 cm. The former open cavity, Figure 1, has dimensions (L,D,W)=(32,38,53) cm. A wooden panel was inserted around the open wall of the cavity to avoid back radiation between the source and the measurement points, Figure 4. A Sonavox Honeycomb loudspeaker (4 “) was formerly set at the centre line of the front wall. This is the open cavity whose acoustic resonances were previously characterized

in the Anechoic Room of the CAEND (Ortiz *et al.*, 2013). This cavity will be used now for the new measurements, introducing some slight modifications.

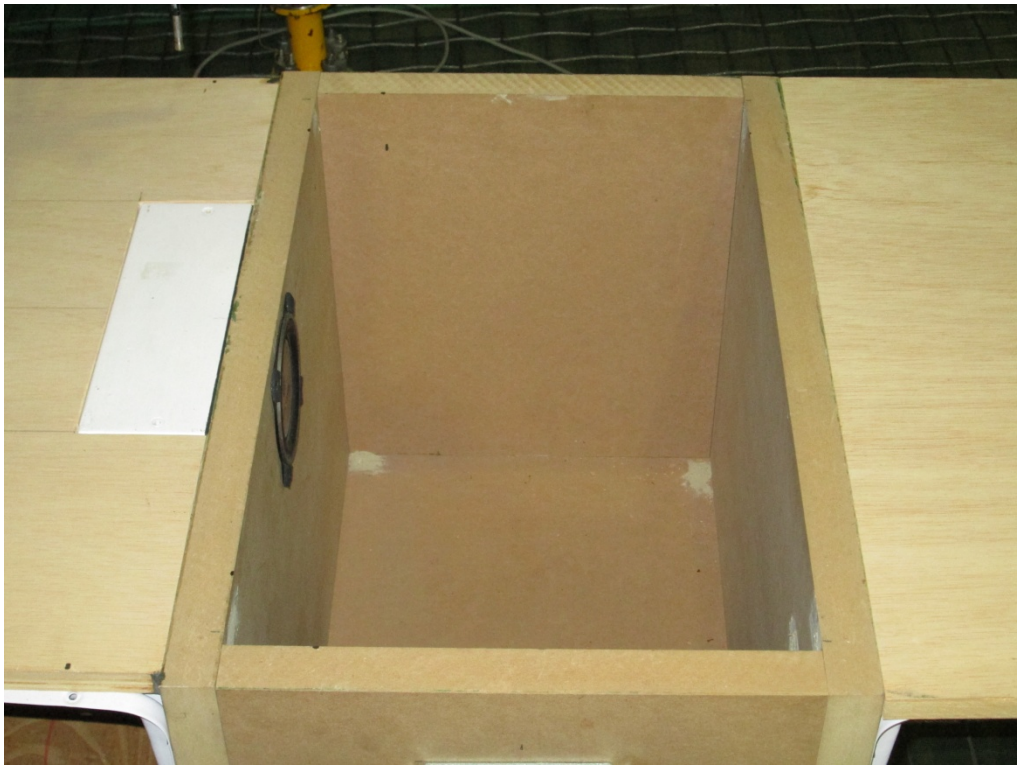

Figure 4. The 3D baffled open cavity

These modifications include:

1. The former 4" loudspeaker will be substituted by the point source described in Section 3.
2. The inner walls of the cavity will be lined with the MPP absorbers described in Section 4.

The FRFs between the point source and a microphone moving across the cavity will be measured by the procedure explained in Section 5.

3. THE POINT SOURCE

Polack *et al.* (2000) proposed an original design for a point and/or omnidirectional source. The Polack design is based on that a small source is a good approximation for an omnidirectional source. Therefore, a large source that radiates through a small opening might be a reasonable implementation of a point source.

We have used this reverse horn design, which consists of a loudspeaker driver mounted on a cylindrical cabinet feeding a small aperture through a reverse horn, to construct the point sources. The acoustic performance of such point source design depends of the following parameters:

1. The volume of the loudspeaker cabinet, V_{rc}.

2. The length of the cone, *L*.

3. The small diameter of the cone, ϕ_s, the large diameter of the cone, ϕ_L, and the loudspeaker Small-Thiele parameters.

A numerical model based on the standard electroacoustic model of a loudspeaker driver, coupled to one or more transmission line segments describing the horn, was used to predict the acoustical performance of the source (Ortiz *et al.*, 2014). As a result of this modelling, it was decided to construct two different configurations both with a 1.5 litter cabinet: a smaller aperture diameter of 7.5 mm and a smaller cone length of 200 mm, and a larger aperture of 15 mm diameter with a longer cone length of 300 mm. Figure 5 shows the drawing of the shorter cone, smaller aperture source.

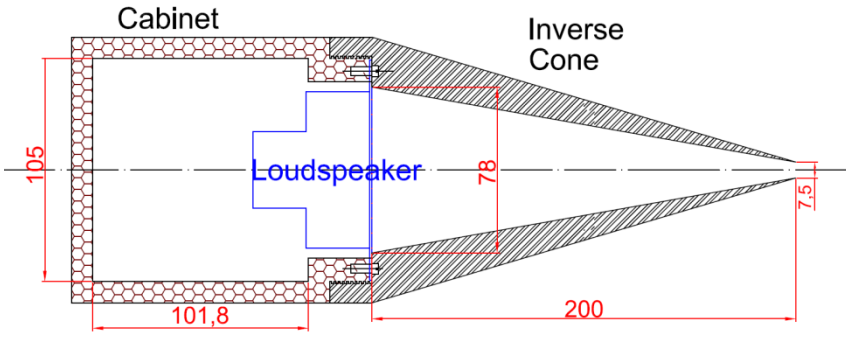

Figure 5. Drawing of the constructed point source proposed (after Ortiz et al., 2014)

Two sources were built with the same design, one of aluminium and other of plastic. We decided to use the plastic source, Figure 6, for measuring the acoustic resonances of the cavity. Since this point source might radiate inside the cavity, a 5 cm large plastic tube of inner diameter 7.5 mm, was coupled to its small aperture.

Figure 6. The plastic source, before (left) and after (right) inserting the shorter cone with smaller aperture

A deleterious effect of the inverted cone is that it produces a lot of resonance peaks in the frequency response of the source. Fortunately, large peaks of the frequency response of a sound source can be equalised by inverse filtering (Cobo *et al.*, 2007; 2013). The design of the inverse filtering requires the measurement of the anechoic frequency response of the source.

In previous applications of inverse filtering, we have seen that, while equalization is perfect on the source axis, its performance degrades slightly out of such axis. Since most of the measurements inside the cavity will be taken out of the source axis, we chose to carry out the inverse filtering with the microphone close to the source and forming a certain angle with its axis, Figure 7. Note the short tube coupled to the small aperture of the point source. A minimum-phase, cosine-amplitude inverse filter was devised with parameters (g,f_1,f_2,C)=(0.04,100 Hz,8 kHz,0.05), being g the exponent of the cosine function, (f_1,f_2) the lower and higher frequencies of the filter amplitude, and C the regularization constant (Cobo *et al.*, 2007). Figure 8 shows the source waveform before and after applying inverse filtering. The drastic shortening of the waveform after applying the inverse filtering is clearly seen in Figure 8. The equalization effect is better appreciated in Figure 9, which shows the source frequency response before and after inverse filtering.

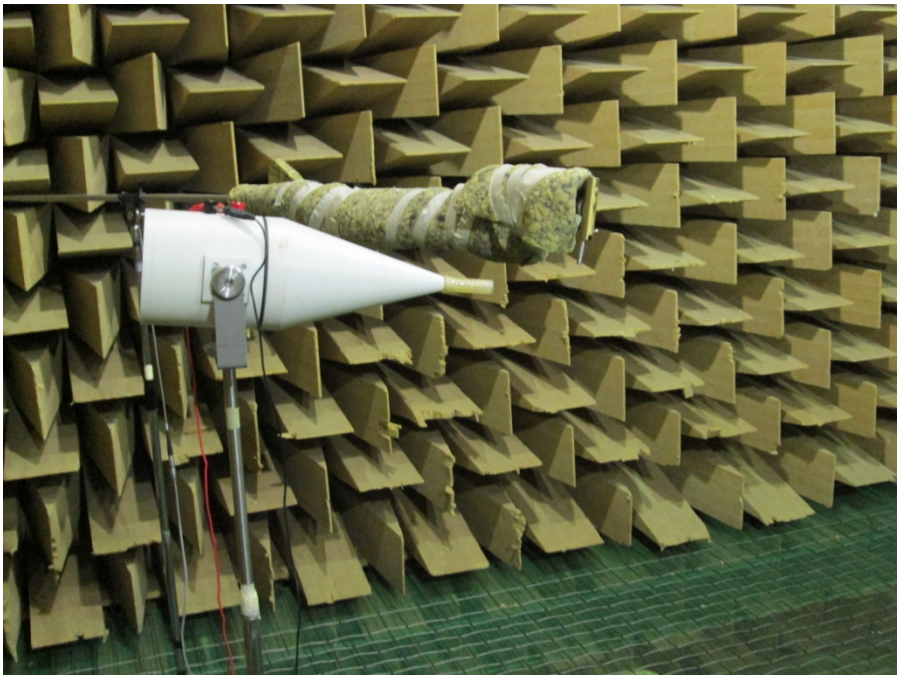

Figure 7. Source-microphone setup for the calculation of the inverse filter

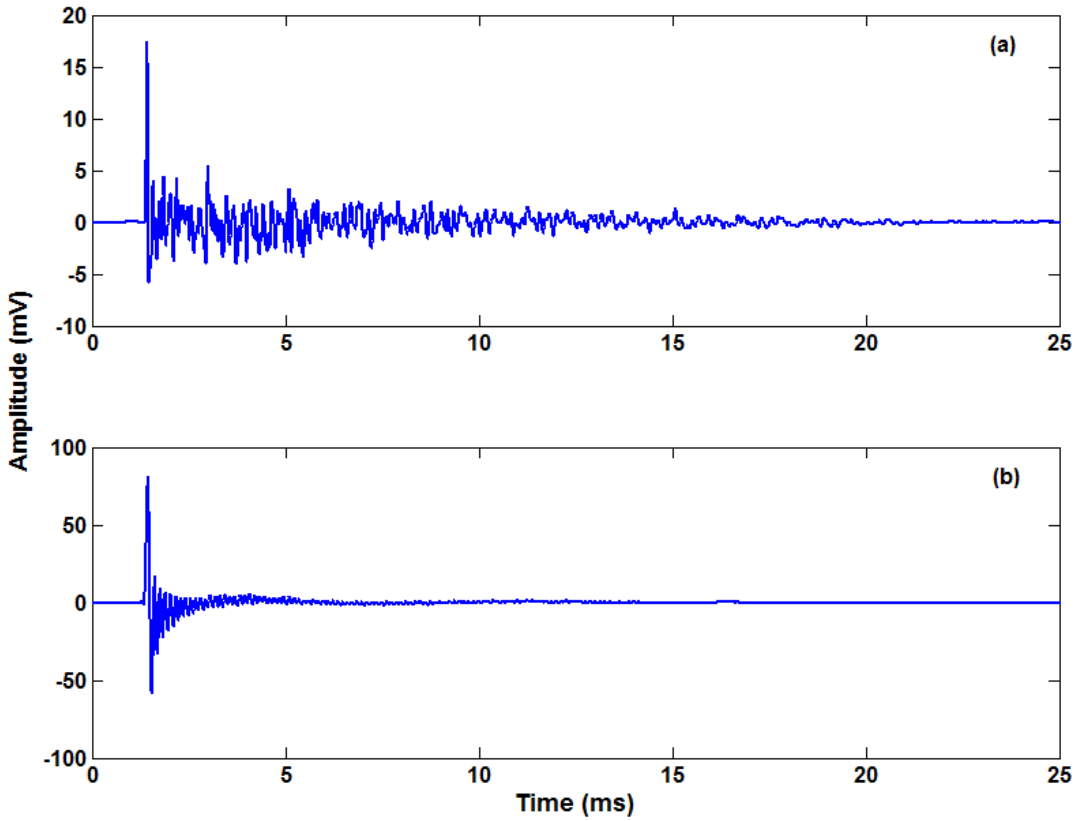

Figure 8. Waveform of the point source, before (a) and after (b) inverse filtering

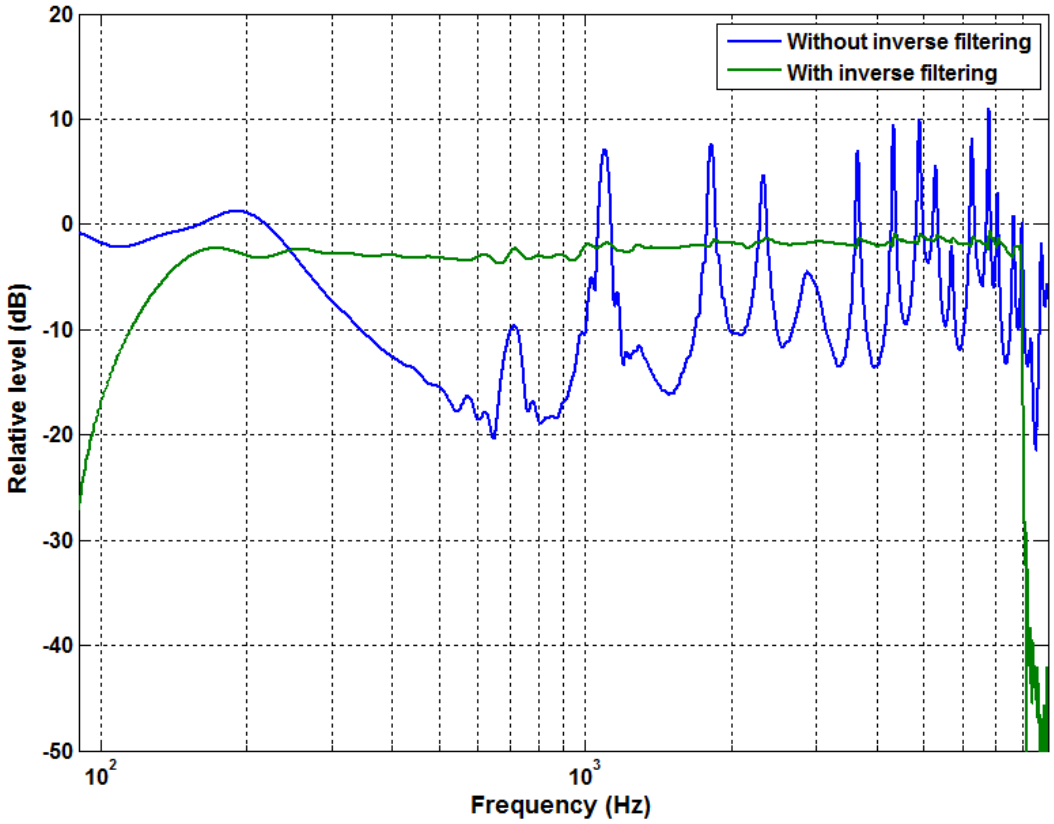

Figure 9. Frequency response of the point source, before and after inverse filtering

4. THE MPP

Several models have been proposed to predict the absorption of MPPs. The pioneer work of Maa (1987; 1998) modelled the input impedance of the MPP including three terms: that of the holes, that of the edges, and the one corresponding to the air cavity. The Maa model provided the following input impedance

$$Z_{Maa} = \frac{\sqrt{2\rho_0\omega\mu}}{2\phi} + i\frac{\omega\rho_0}{\phi}\left\{0.85\,\frac{d}{F(\epsilon)} + t\left[1 - \frac{2}{s\sqrt{-i}}\frac{J_1(s\sqrt{-i})}{J_0(s\sqrt{-i})}\right]^{-1}\right\} - iZ_0 cot(kD)\ , \qquad (1)$$

where (d,t,ϕ,D) are the hole diameter, the panel thickness, the perforation ratio, and the air cavity depth, respectively, μ, ρ_0 y Z_0 are the viscosity, density and characteristic acoustic impedance of the air, respectively, s

$$s = d\sqrt{\frac{\rho_0\omega}{4\mu}}\ , \qquad (2)$$

is the ratio of the hole diameter to the viscous boundary layer, $\epsilon = \sqrt{\phi}$, $F(\varepsilon)$ is the Fok function

$$F(\epsilon) = (1 - 1.4092\,\epsilon + 0.33818\,\epsilon^3 + 0.06793\,\epsilon^5 - 0.02287\,\epsilon^6 + 0.03015\epsilon^7 - 0.01641\epsilon^8)^{-1}, \quad (3)$$

and J_1 and J_0 are the Bessel functions of first class, and order 0 and 1, respectively. Maa (1998) used the approximation of this equation in the range of medium values of *s* to predict the absorption coefficient as a function frequency and the parameters (*d,t,ϕ,D*).

Atalla and Sgard (2007) proposed the equivalent fluid model to characterize the input impedance of an MPP. This model uses the following equation for the input impedance

$$Z_{AS} = i\omega\rho_0\alpha_\infty \left[1 + \frac{\sigma\phi}{i\omega\rho_0\alpha_\infty}\left(1 + i\frac{4\omega\rho_0\mu\alpha_\infty^2}{\sigma^2\phi^2r^2}\right)^{1/2}\right]\frac{t}{\phi} - iZ_0cot(kD) \quad , \quad (4)$$

where

$$\alpha_\infty = 1 + \frac{2\epsilon_e}{t} \quad , \quad (5)$$

is the geometrical tortuosity

$$\epsilon_e = 0.48\sqrt{\pi r^2}\left(1 - 1.14\sqrt{\phi}\right) \quad , \quad (6ª)$$

is the excess of vibrating mass at the hole edges, and

$$\sigma = \frac{32\mu}{\phi d^2}, \quad (7)$$

is the flow resistivity. For squared holes, they propose to use

$$\epsilon_e = 0.48\sqrt{A_{perf}^2}\left(1 - 1.25\sqrt{\phi}\right) \quad , \quad (6b)$$

where A_{perf} is the perforation area. The equivalent fluid model of MPP with circular holes provides the following viscous and thermal characteristic lengths

$$\Lambda = \Lambda' = \frac{d}{2} = r \quad . \quad (8)$$

Both models yield very similar values for the input impedance of a MPP.

One of the main shortcomings to construct an MPP is its high manufacturing cost. Cobo and Montero de Espinosa (2013) proposed an infiltration technique to manufacture cheaper MPPs. The procedure is simpler if *d=t*. The MPPs manufactured by infiltration contain irregular, unevenly distributed perforations. Cobo and Montero demonstrated that the equations of the Maa and equivalent fluid models can be still used whenever the constitutive parameters are slightly modified. Therefore, the equivalent fluid model for a MPP manufactured by infiltration requires modified values for the flow resistivity and geometrical tortuosity given by

$$\sigma = s_\sigma \frac{32\mu}{\phi d^2} \quad , \tag{9}$$

$$\alpha_\infty = s_{\alpha\infty}\left(1 + \frac{2\epsilon_e}{t}\right) \quad . \tag{10}$$

The modified equivalent fluid model has been used to design MPPs for lining the inner walls of the open cavity. Two MPPs were designed to cover the frequency range between roughly 700 and 2000 Hz.

The proposed MPPs have the parameters summarized in Table 2. Figure 10 shows the normal incidence absorption curves for both MPPs for D=2 cm, and (s_σ,$s_{\alpha\infty}$)=(1.4, 0.7). The MPP1 has a half absorption band of (670, 1310) Hz, centred at 920 Hz. The MPP2 absorbs in the frequency band (728, 1623) Hz, centred at 1073 Hz.

Table 2. Parameters for the two proposed MPPs

MPP	d (mm)	t (mm)	ϕ (%)
MPP1	0.55	0.55	0.50
MPP2	0.4	0.4	0.52

Several samples of both MPP1 and MPP2 were manufactured. Figure 11 shows a picture of one of the manufactured MPPs.

Then, the inner walls of the open cavity described in Section 2 were lined with samples of both MPPs according to a patchwork pattern. Figure 12 shows two pictures of the lining process. The final lined cavity is shown in Figure 13.

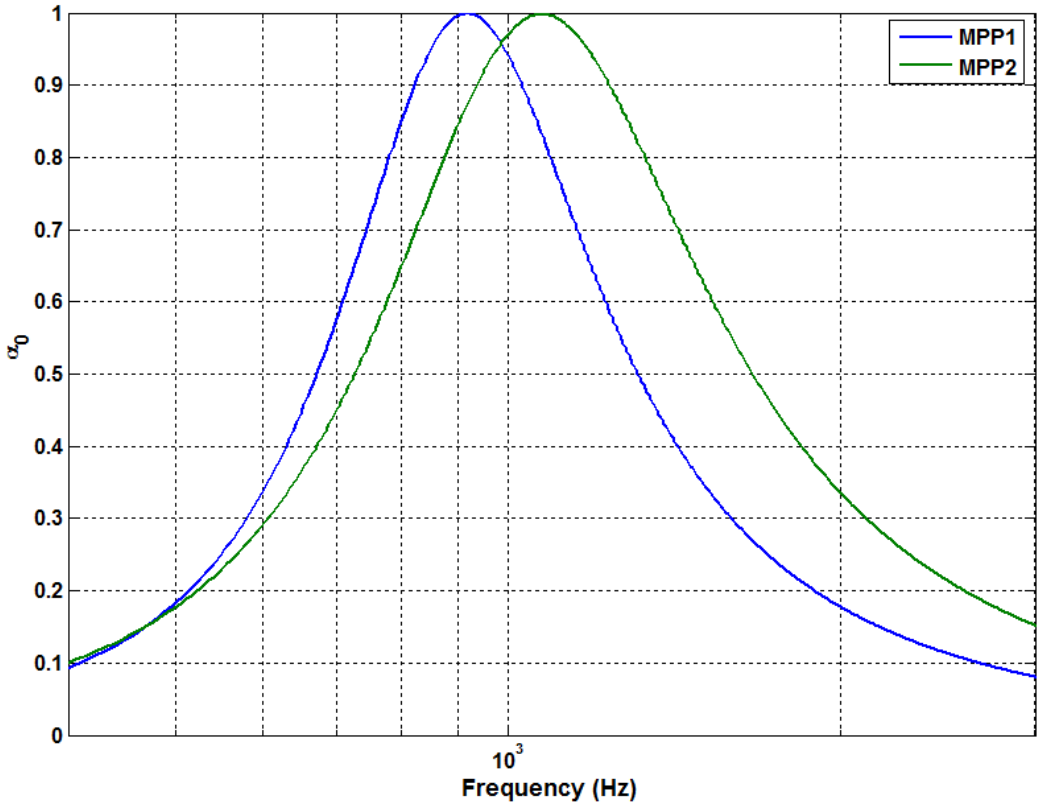

Figure 10. Normal incidence absorption coefficients for the two MPPs for D=2 cm, and $(s_\sigma s_{\alpha\infty})=(1.4,0.7)$

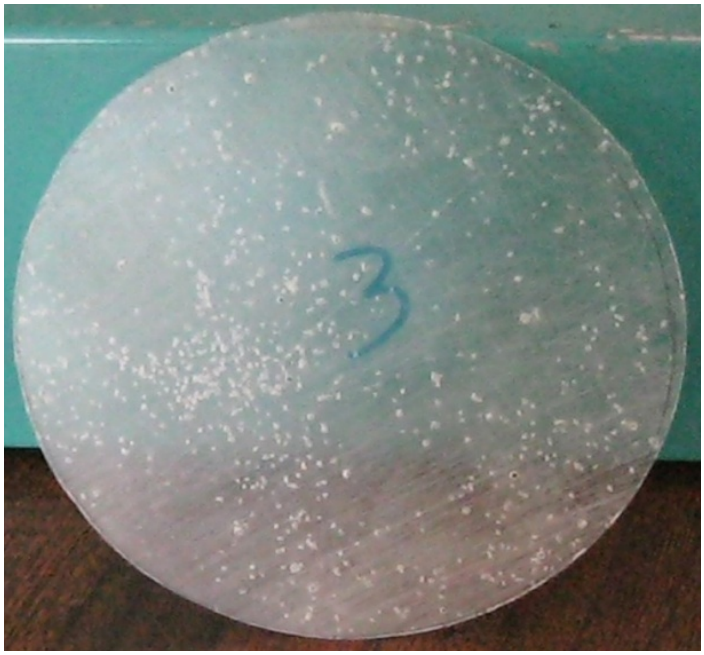

Figure 11. A sample of the MPP manufactured by infiltration

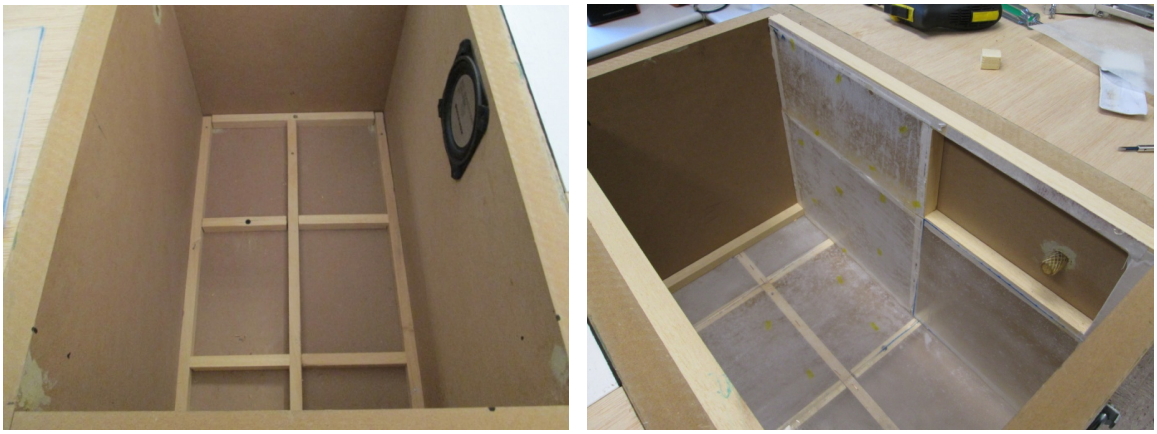

Figure 12. Two pictures of the cavity lining with MPPs procedure

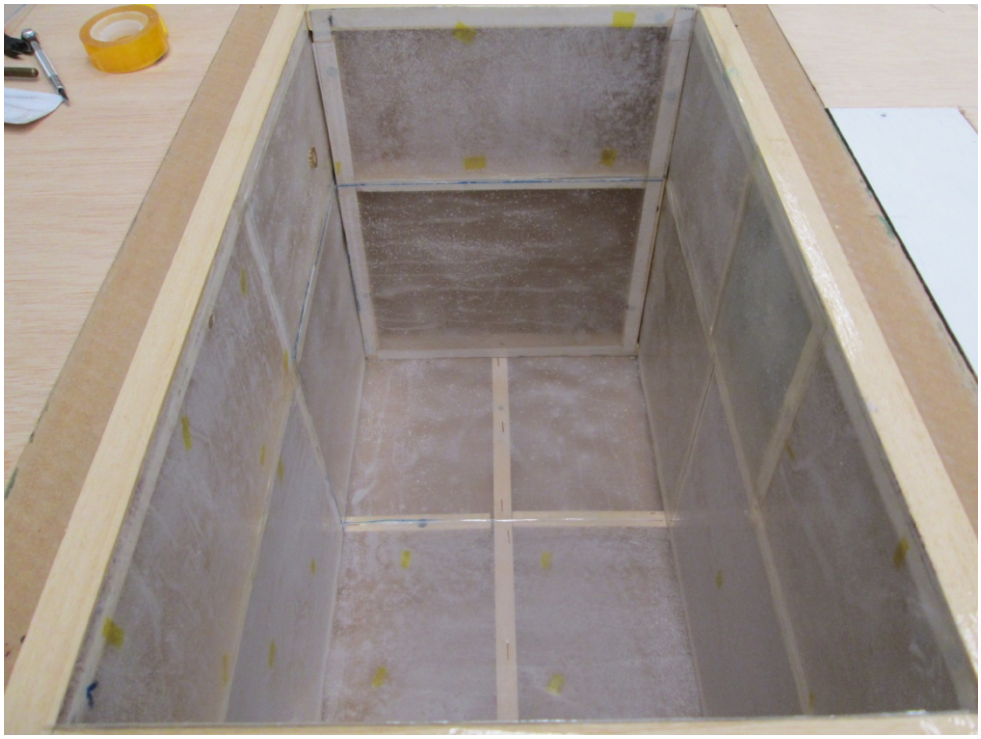

Figure 13. The open cavity lined with MPPs

5. MEASUREMENTS

The measurement system, Figure 14, provides the time responses between the fixed source and a B&K 4939-A microphone moving across the cavity. The measurements are carried out by the self-design Virtual Instrument IMAS-EPE, which drives a NI DAQ PCI-MIO-16E board to acquire the time responses. An order 18 MLS signal drives the source through an amplifier PIONEER A-290R. The acoustic signal radiated by the source is picked up by the microphone and conditioned by a B&K 5935L. The cross correlation between the MLS signal and that picked up by the microphone provides the time response. Since the microphone has flat frequency response and the source has been inverse filtered, the time response is essentially the impulse

response of the cavity. The Fourier transform of the impulse response gives the FRF of the cavity.

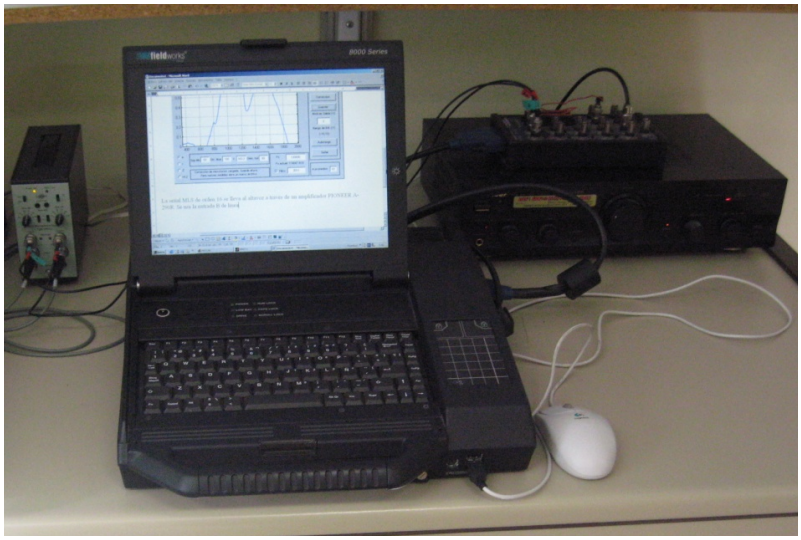

Figure 14. Measurement system for the impulse response pairs

Assuming a Cartesian coordinates system with origin at the centre of the cavity, the source is located at $(x_s,y_s,z_s)=(-0.195,-0.16,0.1)$. The impulse responses were measured at 37 points in the cavity. The points were chosen so that they can be accessed both with the unlined and lined cavities. Therefore, they are closer to the cavity walls in the case of the lined cavity. 18 points are evenly distributed along two x-lines, Figure 15, with coordinates summarised in Table 3, close to the wall opposite to that containing the source.

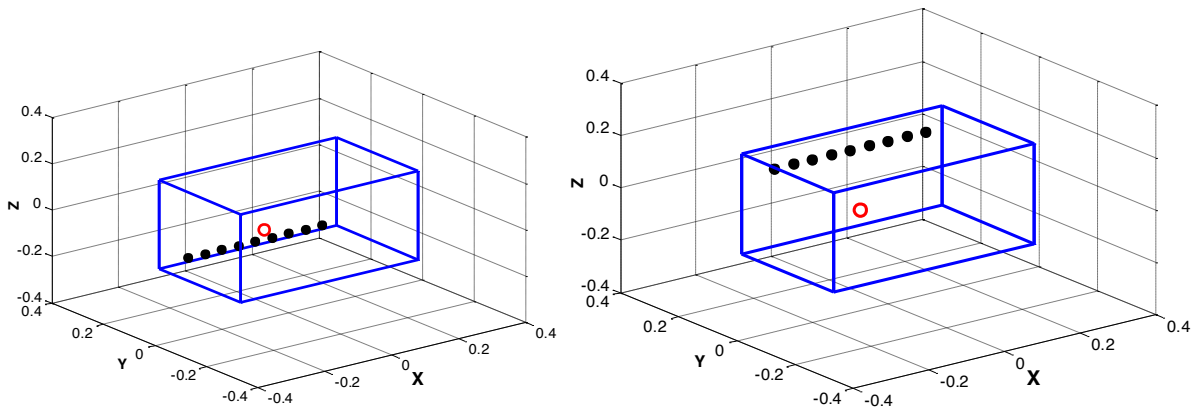

Figure 15. Measurement points along the lower and upper x-lines

Table 3. Coordinates of the measurement points along the lower and upper x-lines

Lower line points	X	Y	Z	Upper line points	X	Y	Z
1	-0,215	0,11	-0,14	10	-0,215	0,11	0,14
2	-0,165	0,11	-0,14	11	-0,165	0,11	0,14
3	-0,115	0,11	-0,14	12	-0,115	0,11	0,14
4	-0,065	0,11	-0,14	13	-0,065	0,11	0,14

5	-0,015	0,11	-0,14	14	-0,015	0,11	0,14
6	0,035	0,11	-0,14	15	0,035	0,11	0,14
7	0,085	0,11	-0,14	16	0,085	0,11	0,14
8	0,135	0,11	-0,14	17	0,135	0,11	0,14
9	0,185	0,11	-0,14	18	0,185	0,11	0,14

Other 10 points are on two y-lines close to the lateral wall farther from the wall containing the source, Figure 16. Table 4 summarises the coordinates of each these 10 points. Notice that points 19 and 24 in Table 4 are redundant with points 9 and 18, respectively in Table 3.

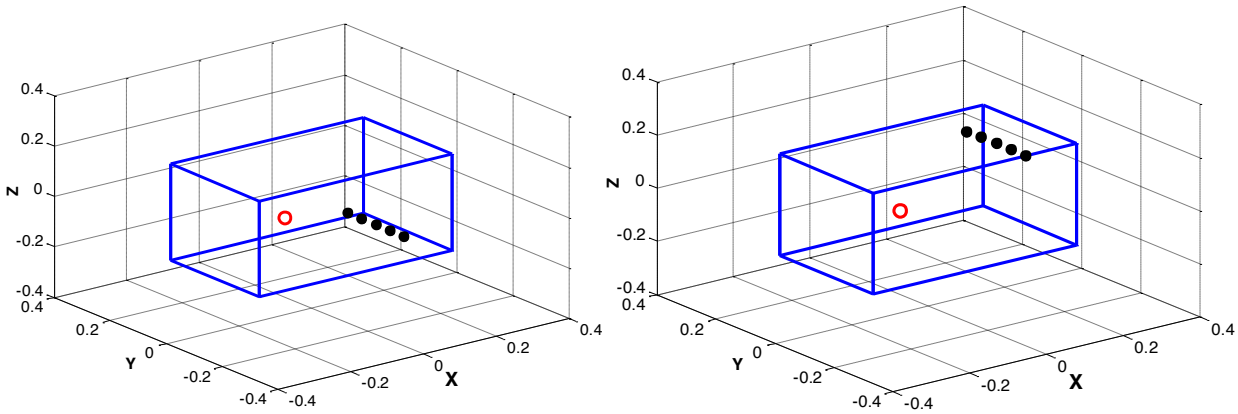

Figure 16. Measurement points along the lower and upper y-lines

Table 4. Coordinates of the measurement points along the lower and upper y-lines

Lower line points	**X**	**Y**	**Z**	**Upper line points**	**X**	**Y**	**Z**
19	0,185	0,11	-0,14	24	0,185	0,11	0,14
20	0,185	0,06	-0,14	25	0,185	0,06	0,14
21	0,185	0,01	-0,14	26	0,185	0,01	0,14
22	0,185	-0,04	-0,14	27	0,185	-0,04	0,14
23	0,185	-0,09	-0,14	28	0,185	-0,09	0,14

Finally, other 9 points outside the cavity, above the upper baffle opposite to the wall containing the source, Figure 17, have been chosen for measuring the impulse responses. Table 5 shows the coordinates of these 9 points.

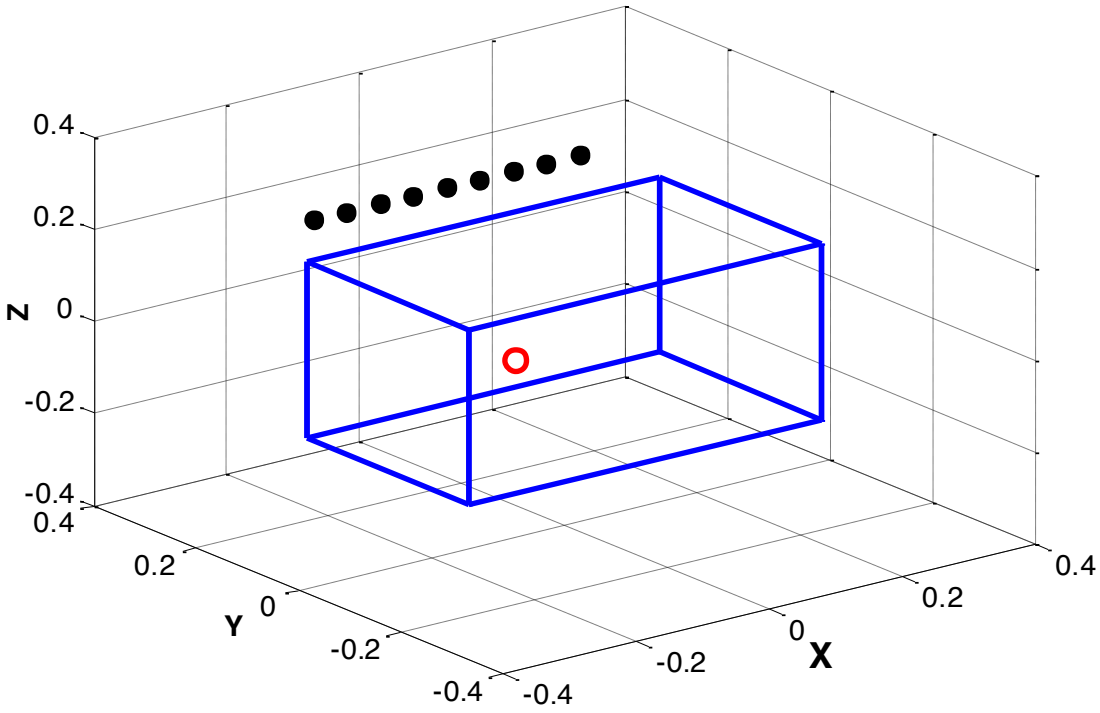

cd

Figure 17. Measurement points along the outer x-line

Table 5. Coordinates of the measurement points along the outer x-line

Line points	X	Y	Z
29	-0,215	0,21	0,24
30	-0,165	0,21	0,24
31	-0,115	0,21	0,24
32	-0,065	0,21	0,24
33	-0,015	0,21	0,24
34	0,035	0,21	0,24
35	0,085	0,21	0,24
36	0,135	0,21	0,24
37	0,185	0,21	0,24

6. RESULTS

The atmospheric conditions during the measurements are summarised in Table 6.

Table 6. Atmospheric conditions during measurements

	Temperature (ºC)	Relative Humidity (%)	Pressure (mb)
Without MPPs	16	34	949,3
With MPPS	15,6	38	949,7

Figures 18-26 show the FRFs at the 9 points along the lower x-line of Figure 15. As it can be seen, the main effect of the MPP lining is to decrease in 10-15 dB the resonances of the cavity in the frequency range from 800 Hz to 3000 Hz. At lower frequencies, the MPP lining can either decrease (Figures 18, 19, 20, 21) or increase (Figures 23, 24, 25, 26) some of the peaks of the FRFs. Figures 27-35 show the corresponding FRFs at the 9 points along the upper x-line of Figure 15. The effect of the MPP lining along these points is less noticeable than that at the points along the lower x-line. At points 10, 11 and 12, there can be seen regions where the peaks either decrease or increase, after lining the inner wall with MPPs. At points 13-18, however, the attenuation of the peaks in the frequency range from 800 to 300 Hz is much more evident. Again, at frequencies lower than 800 Hz, some of the peaks decrease while some others increase.

Figures 36-40 show the FRFs at the points along the lower y-line of Figure 16. The attenuation of the MPP liner is much more noticeable at the inner points of the line (points 20-22), and is lower at the extreme points (points 19 and 23). Some of the peaks are reduced more than 35 dB (see the peaks at around 1100-1200 Hz in Figure 38). However, peaks at roughly 700-750 Hz are intensified about 15 dB. A similar behaviour is observed at the points of the upper y-line, Figures 41-45.

Finally, Figures 46-54 show the FRFs at the points in the line outside the cavity of Figure 17, above one of the baffles surrounding the open surface of the cavity. A similar performance of the MPP liners can be noticed at these points. Namely, a noticeable magnitude reduction in the frequency range where the MPPs were designed to provide sound absorption, and reduction of some peaks and increase of others at frequencies below 800 Hz.

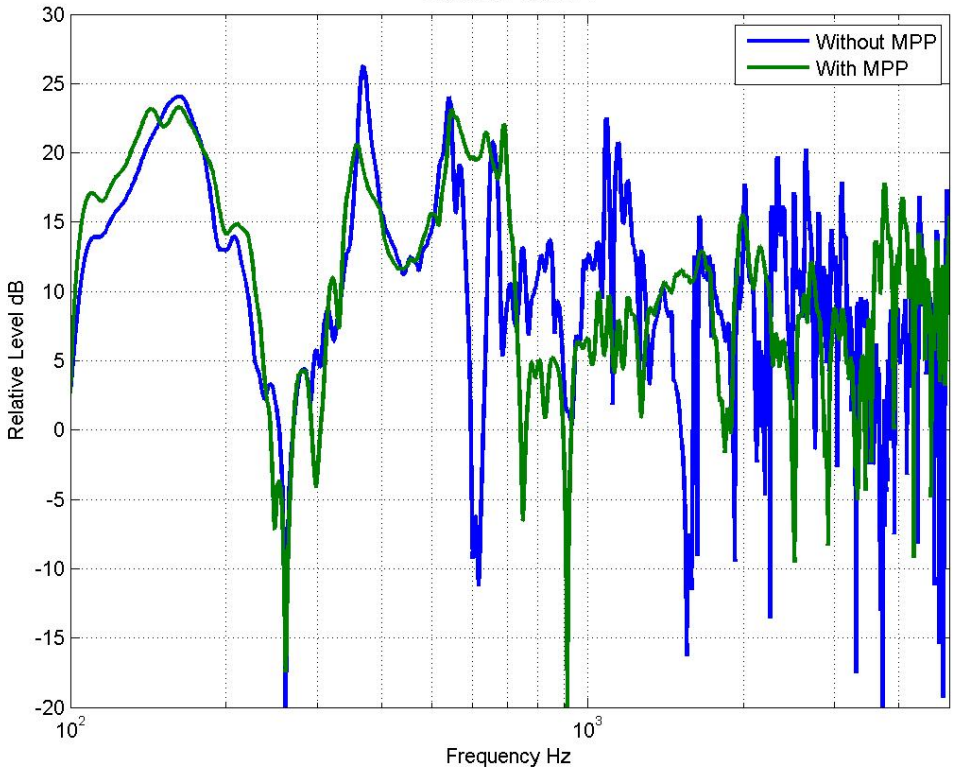

Figure 18. FRF, with and without MPP lining, at the point 1 along the lower x-line

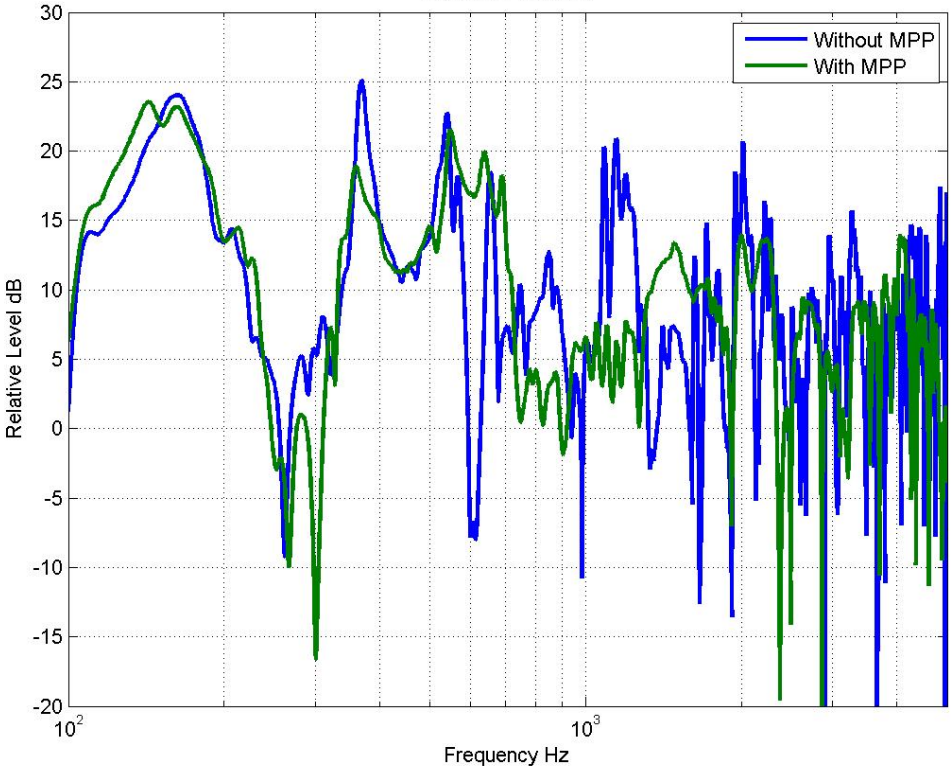

Figure 19. FRF, with and without MPP lining, at the point 2 along the lower x-line

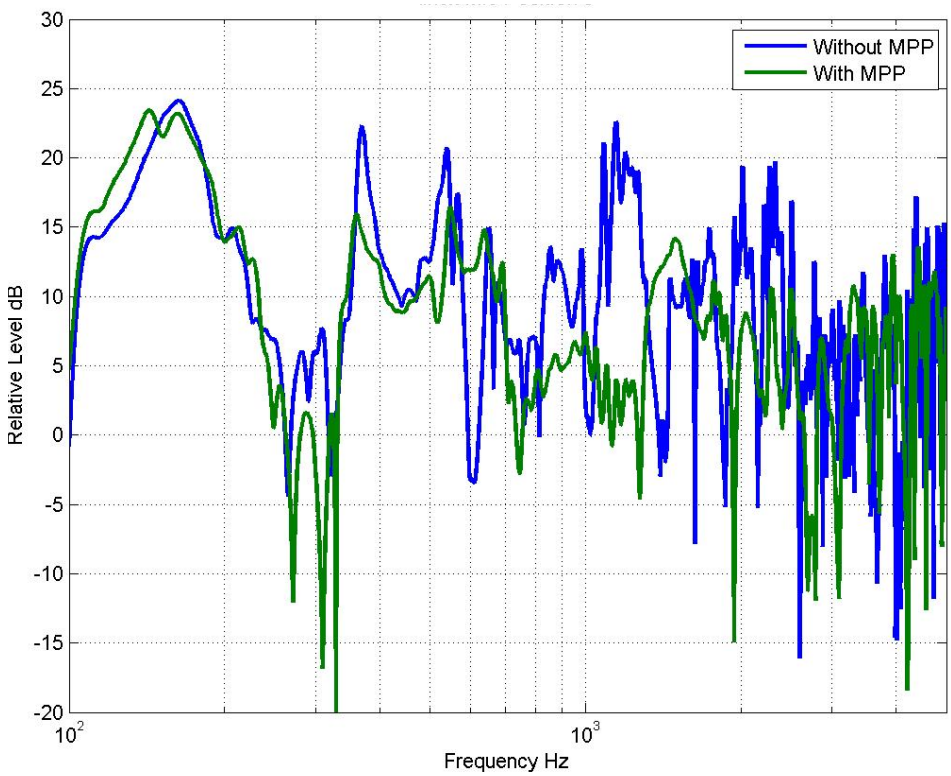

Figure 20. FRF, with and without MPP lining, at the point 3 along the lower x-line

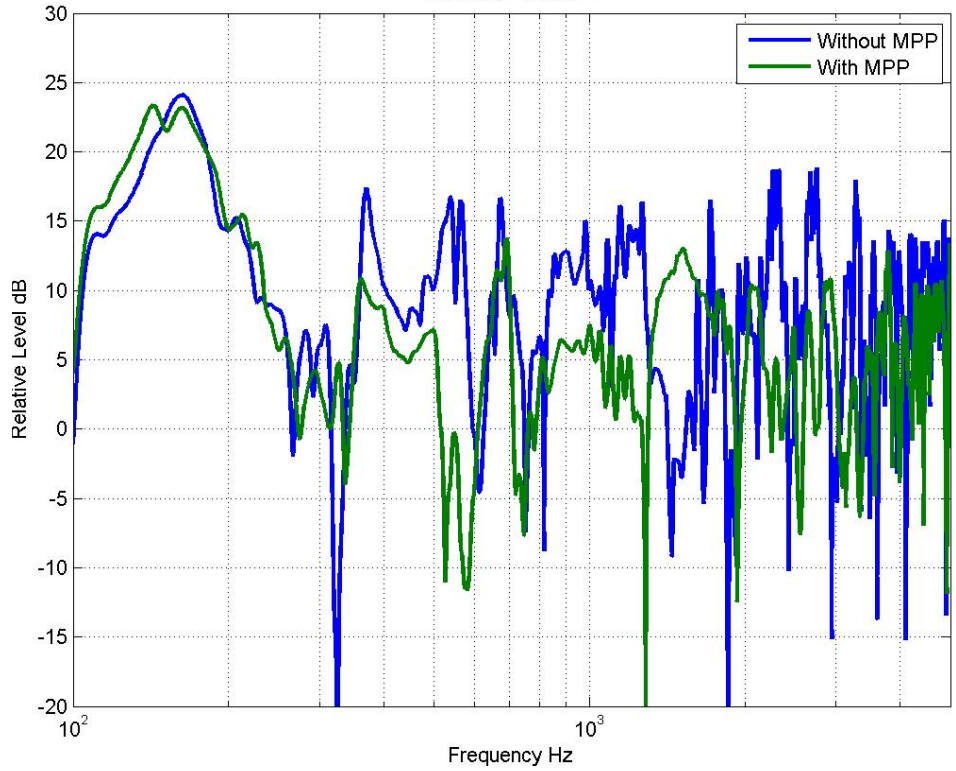

Figure 21. FRF, with and without MPP lining, at the point 4 along the lower x-line

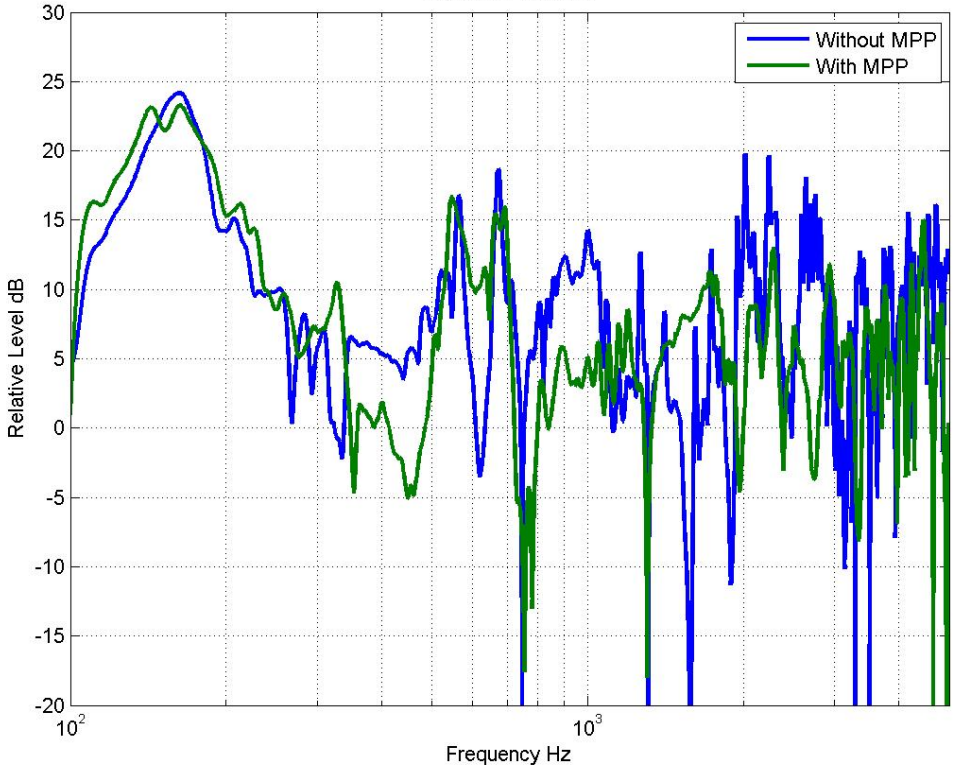

Figure 22. FRF, with and without MPP lining, at the point 5 along the lower x-line

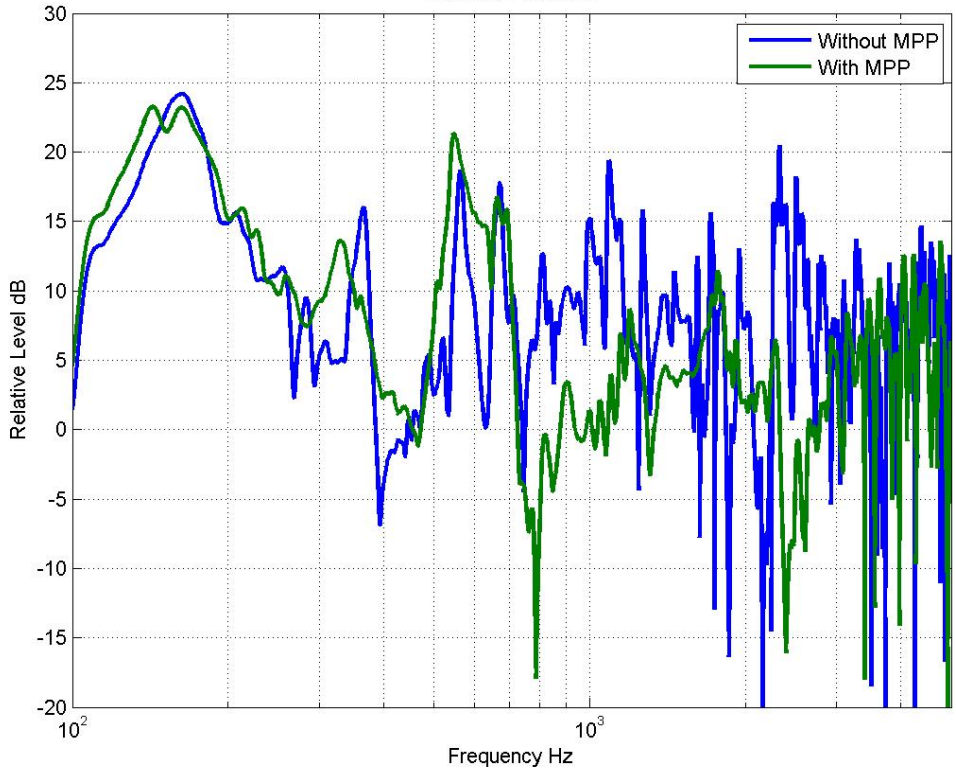

Figure 23. FRF, with and without MPP lining, at the point 6 along the lower x-line

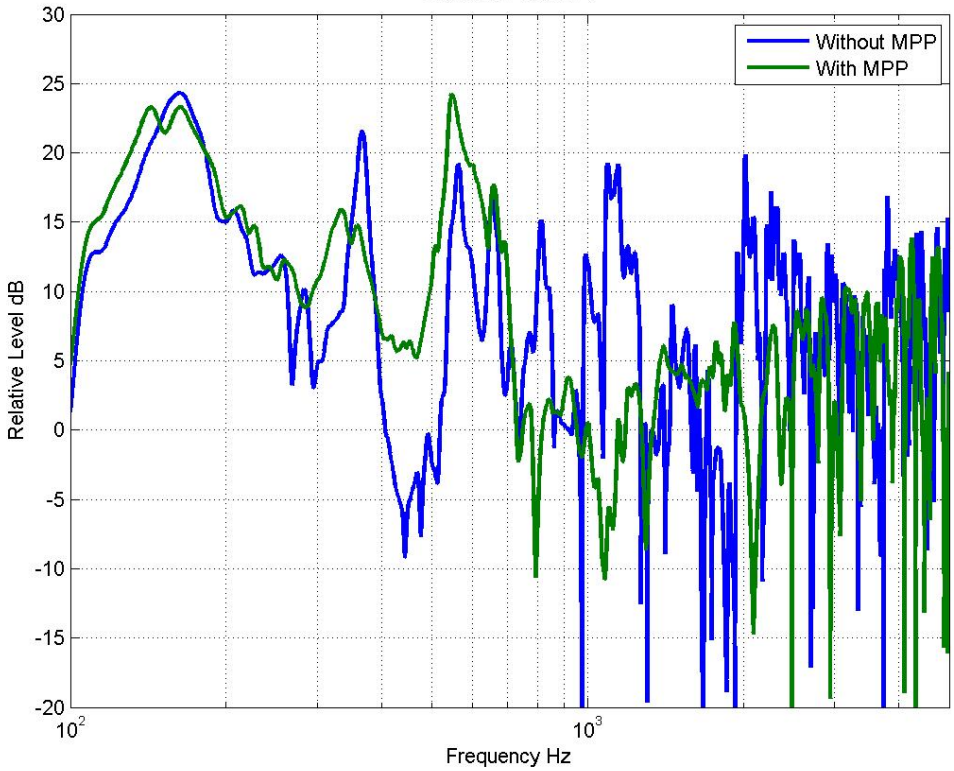

Figure 24. FRF, with and without MPP lining, at the point 7 along the lower x-line

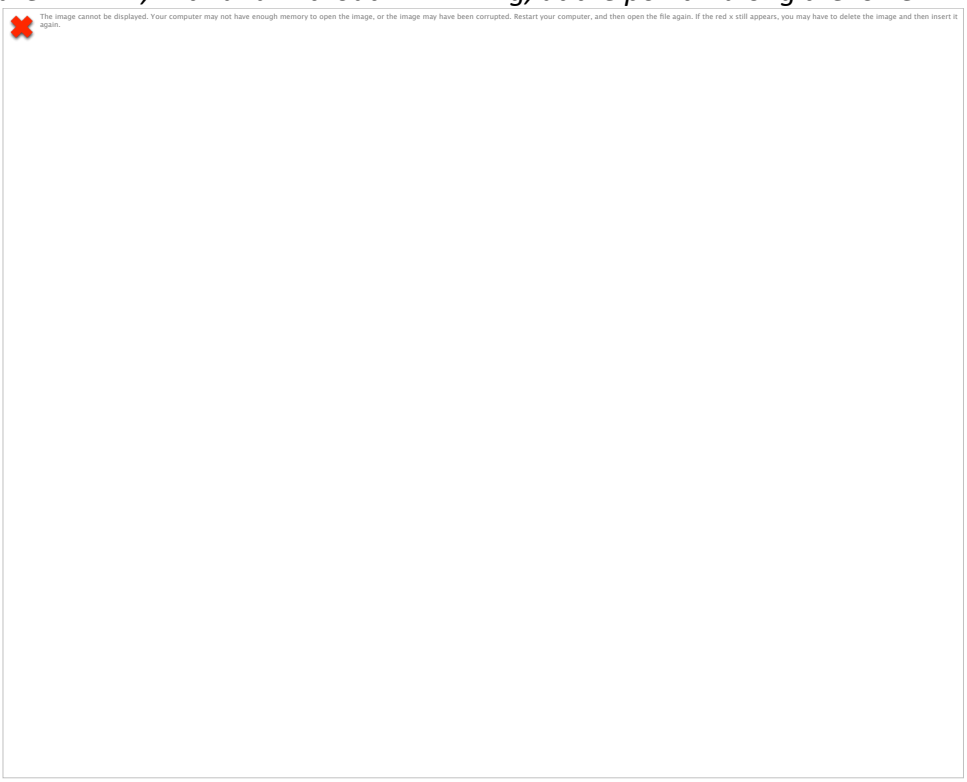

Figure 25. FRF, with and without MPP lining, at the point 8 along the lower x-line

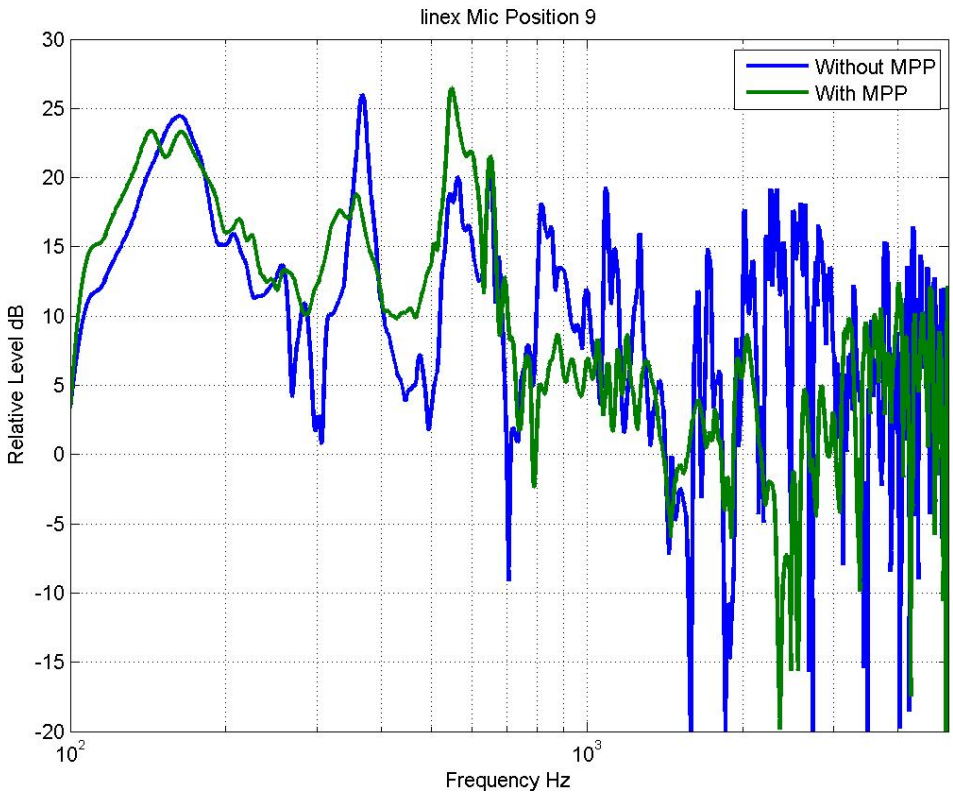

Figure 26. FRF, with and without MPP lining, at the point 9 along the lower x-line

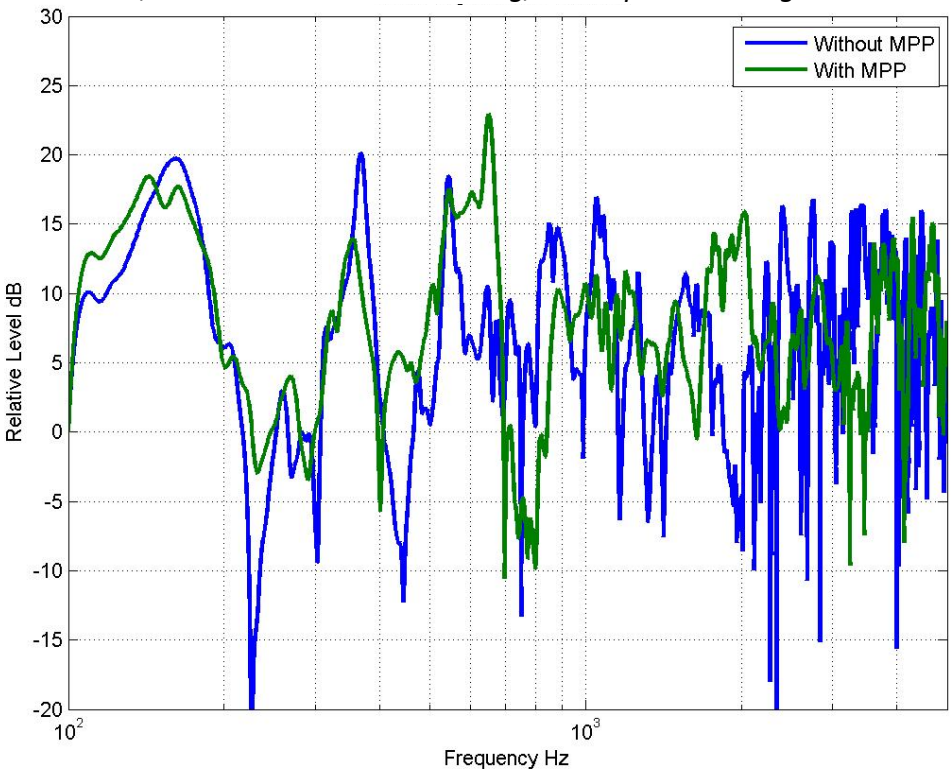

Figure 27. FRF, with and without MPP lining, at the point 10 along the upper x-line

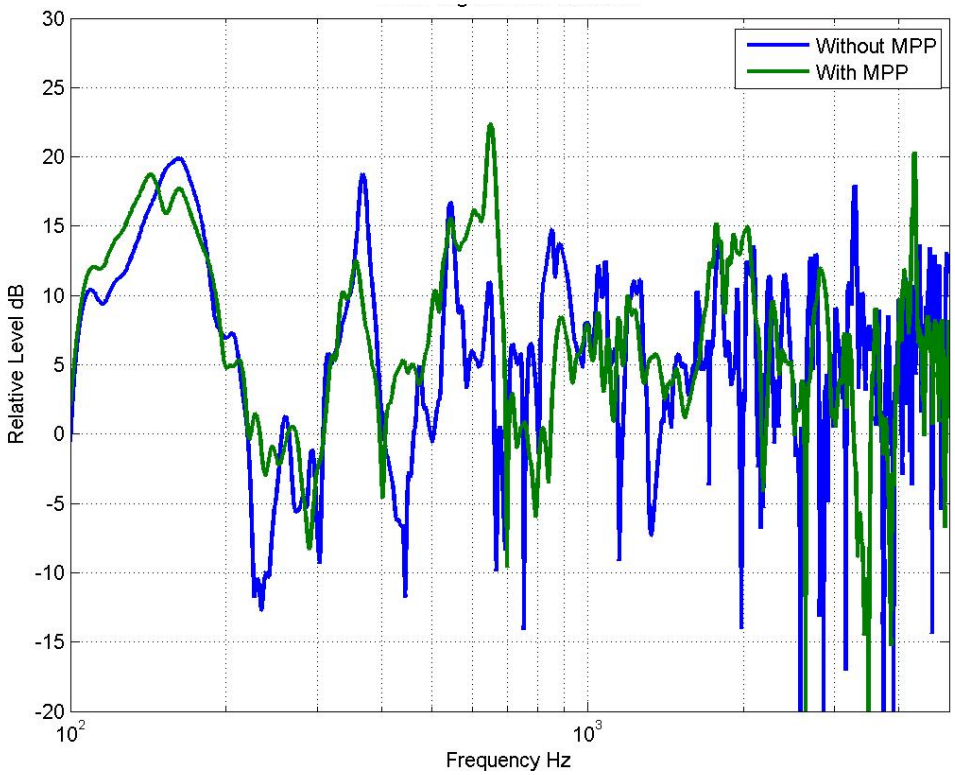

Figure 28. FRF, with and without MPP lining, at the point 11 along the upper x-line

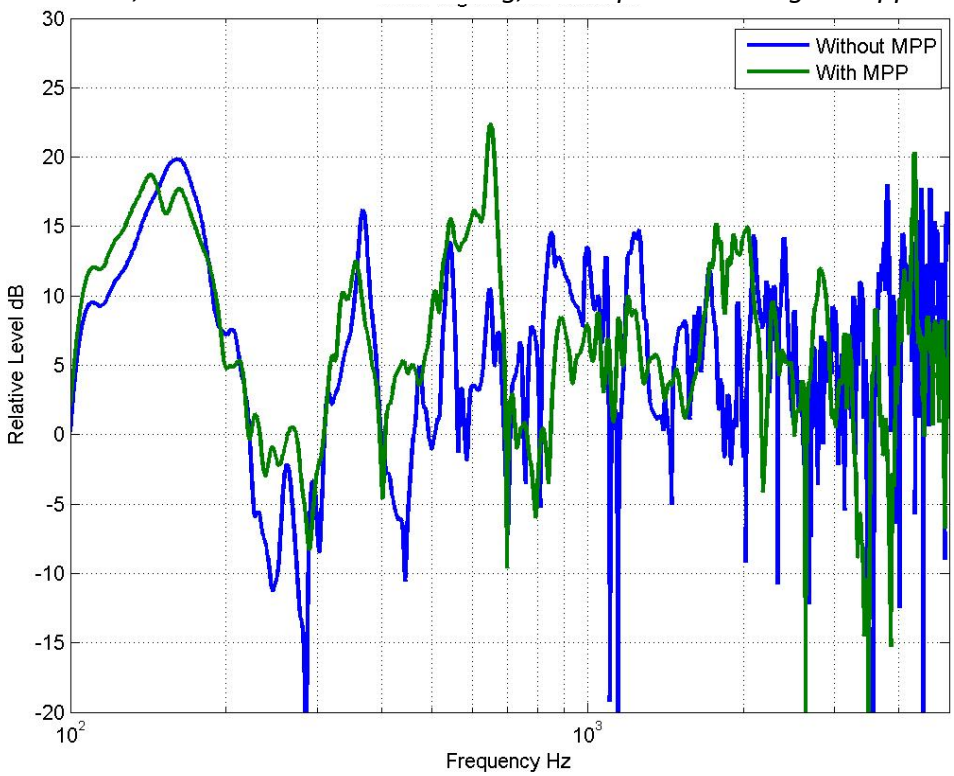

Figure 29. FRF, with and without MPP lining, at the point 12 along the upper x-line

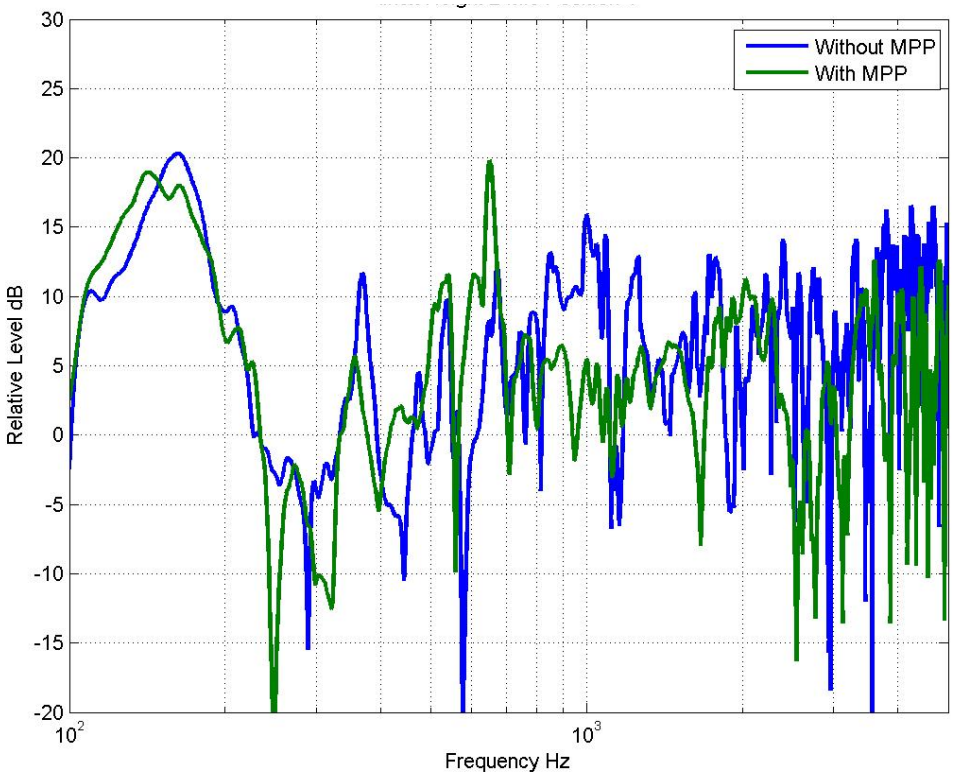

Figure 30. FRF, with and without MPP lining, at the point 13 along the upper x-line

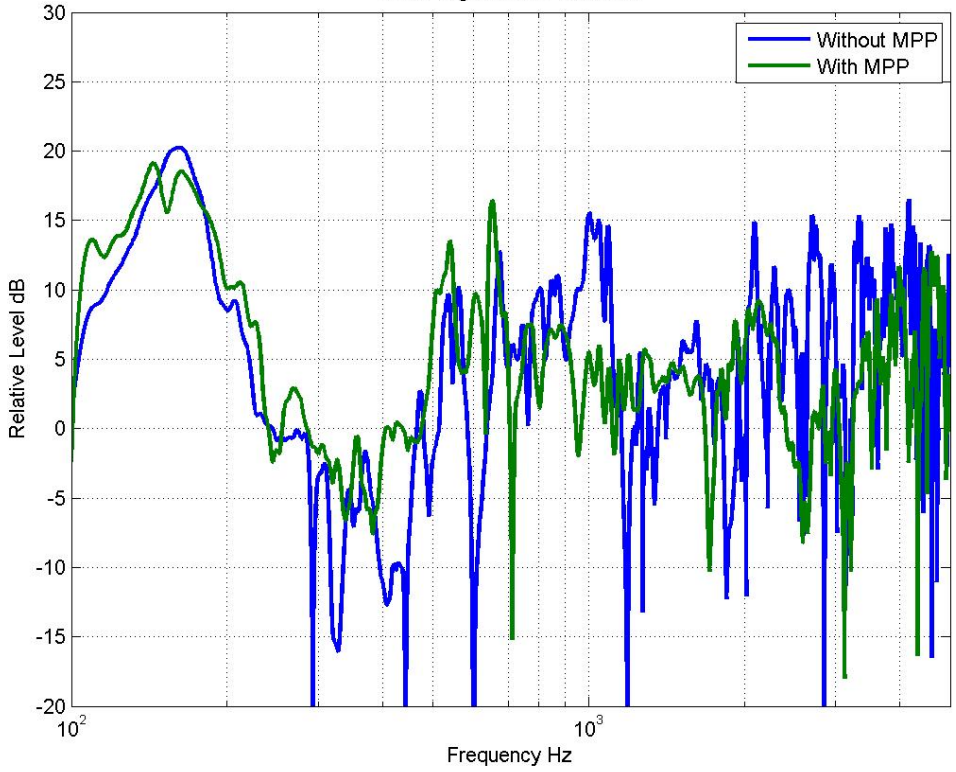

Figure 31. FRF, with and without MPP lining, at the point 14 along the upper x-line

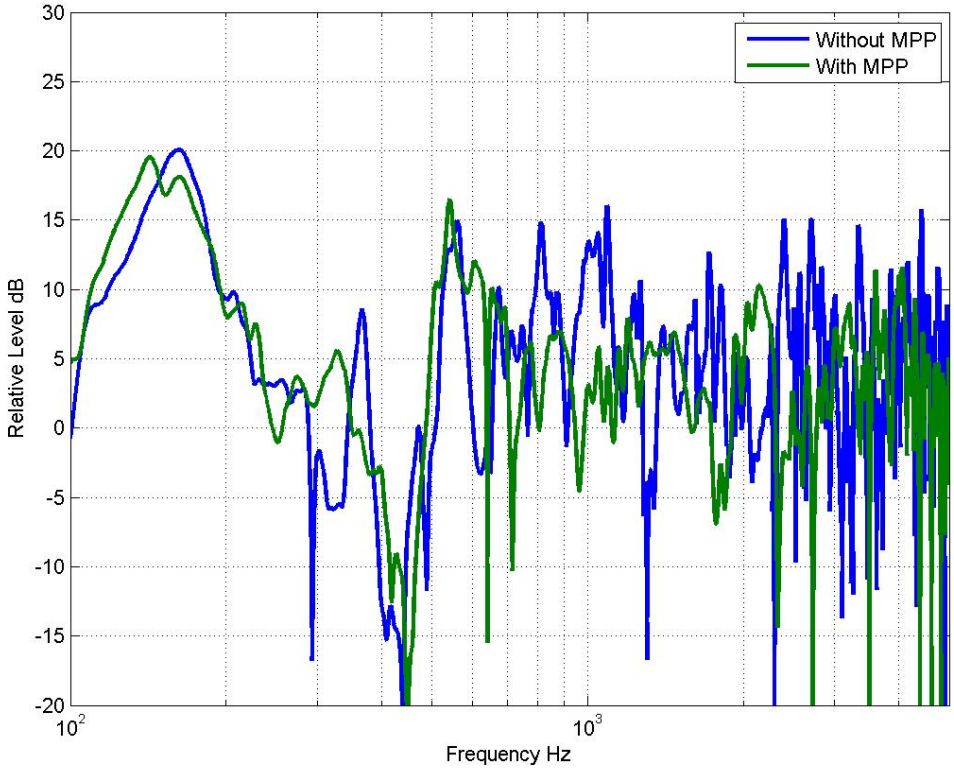

Figure 32. FRF, with and without MPP lining, at the point 15 along the upper x-line

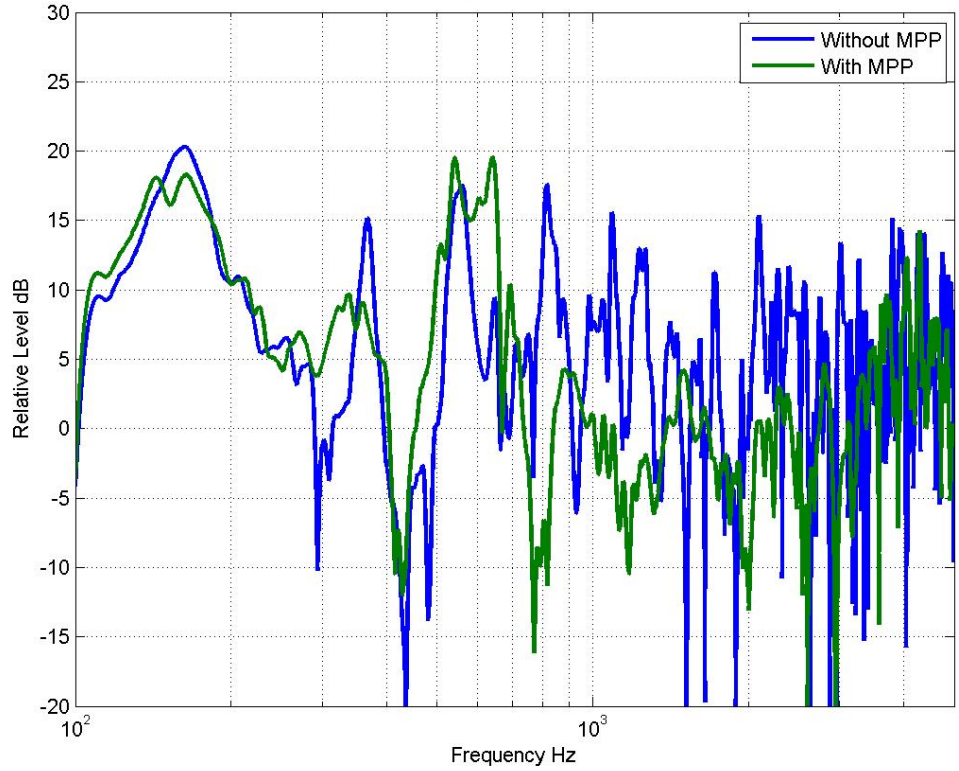

Figure 33. FRF, with and without MPP lining, at the point 16 along the upper x-line

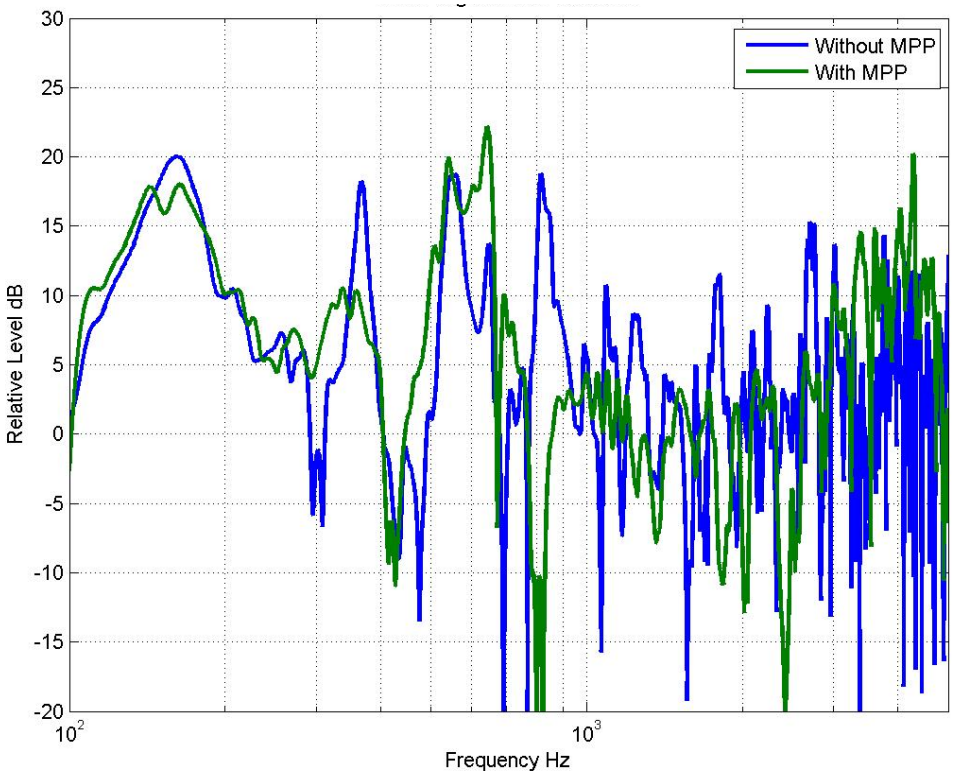

Figure 34. FRF, with and without MPP lining, at the point 17 along the upper x-line

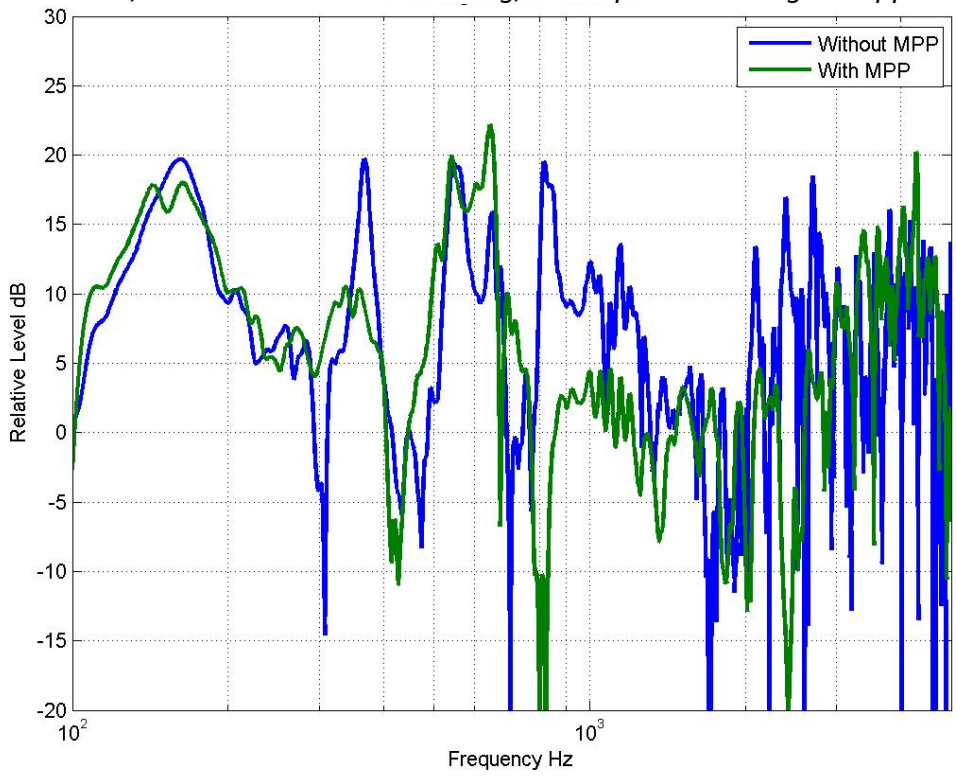

Figure 35. FRF, with and without MPP lining, at the point 18 along the upper x-line

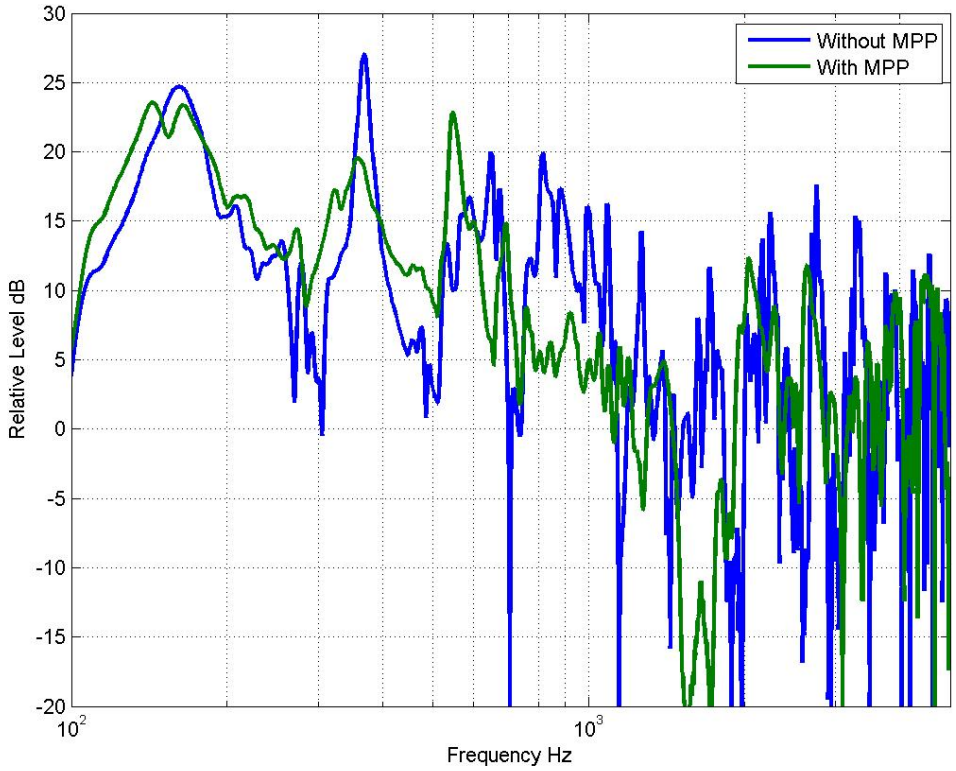

Figure 36. FRF, with and without MPP lining, at the point 19 along the lower y-line

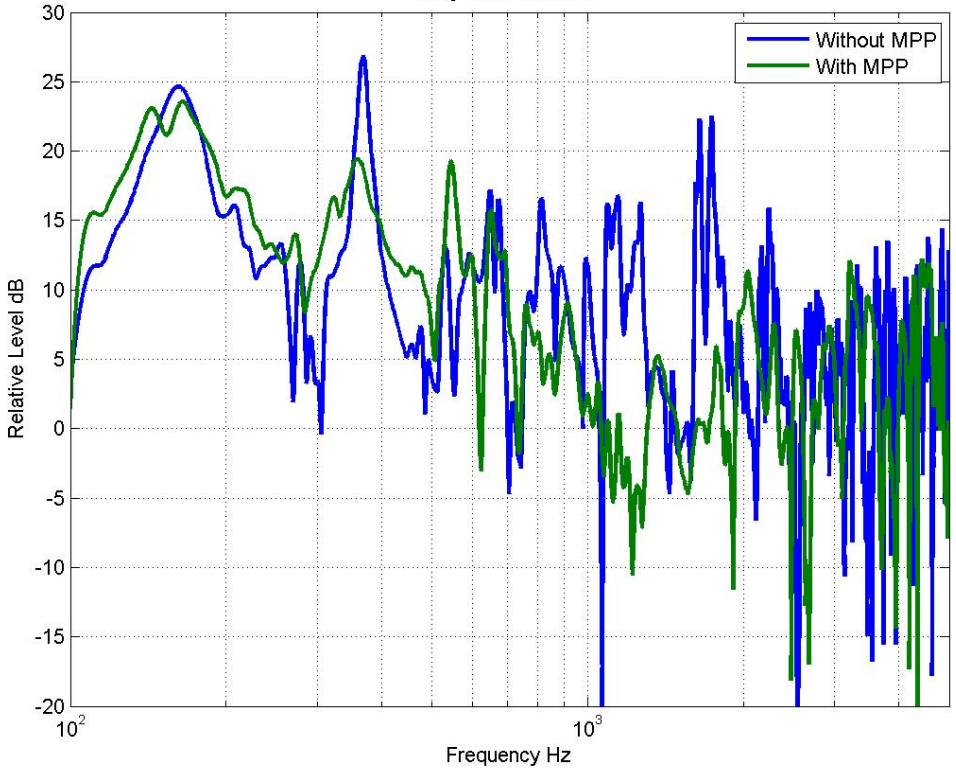

Figure 37. FRF, with and without MPP lining, at the point 20 along the lower y-line

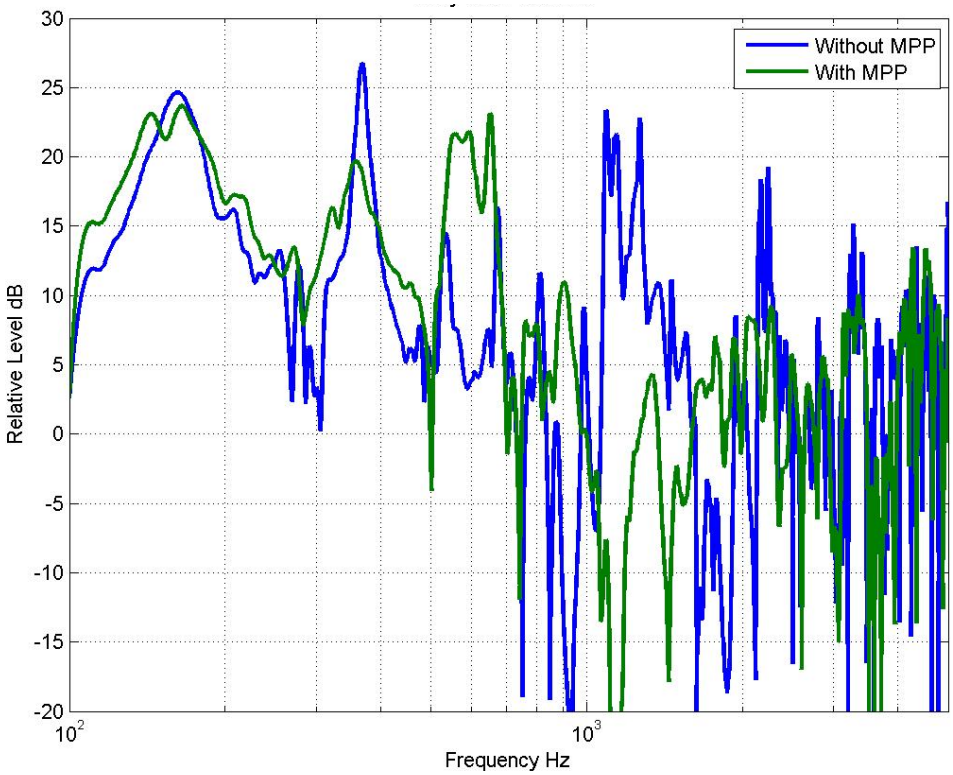

Figure 38. FRF, with and without MPP lining, at the point 21 along the lower y-line

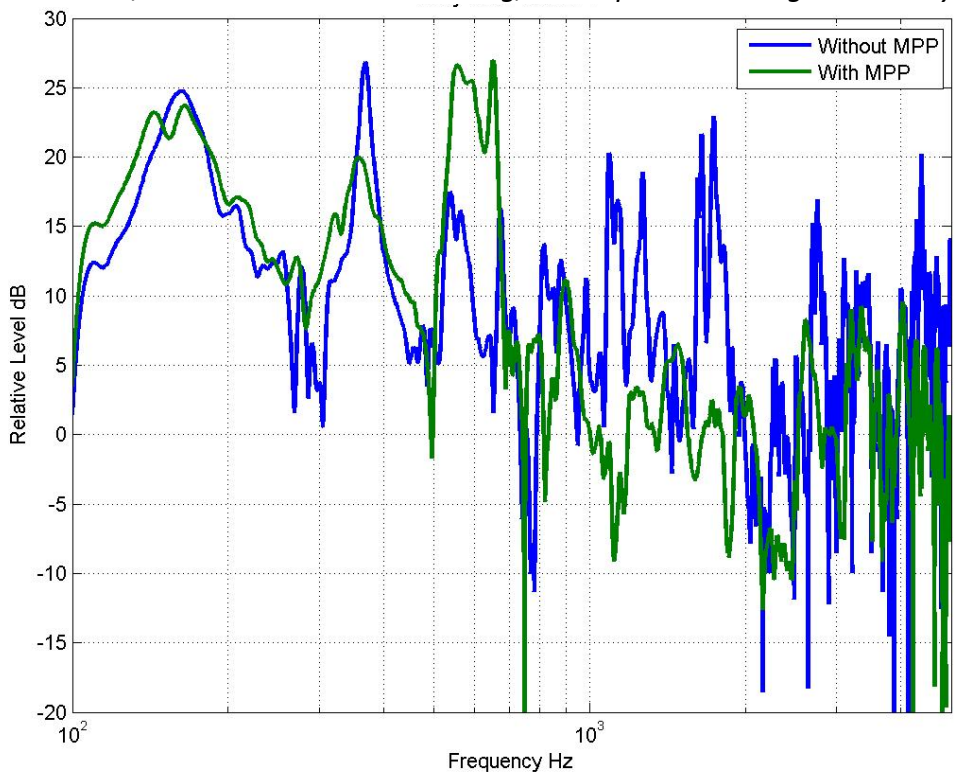

Figure 39. FRF, with and without MPP lining, at the point 22 along the lower y-line

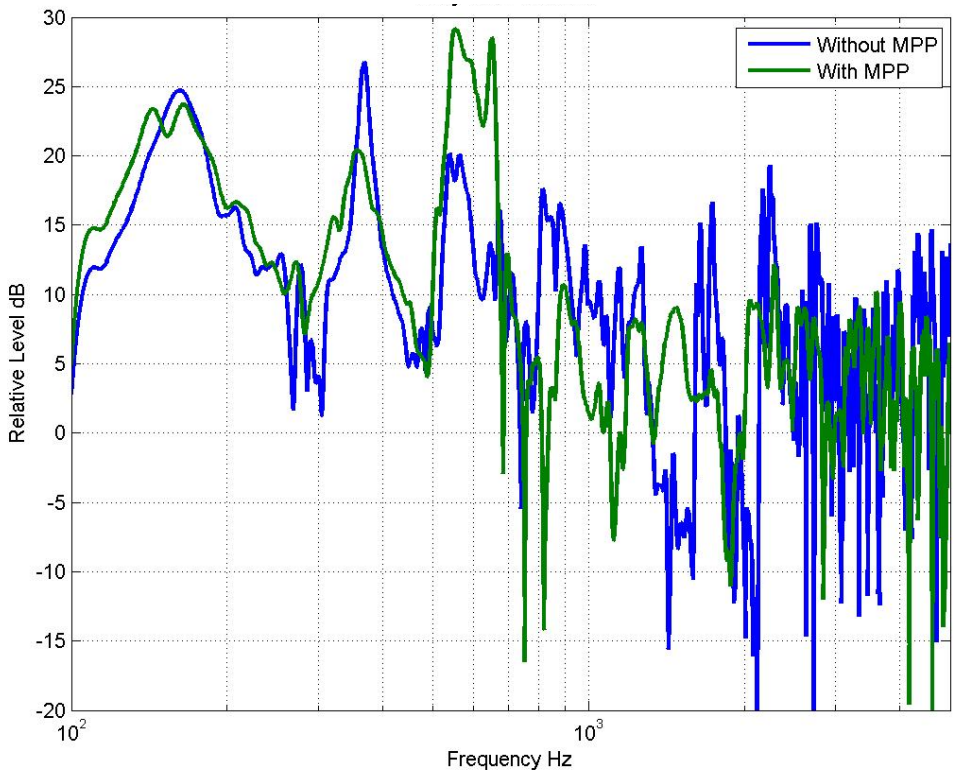

Figure 40. FRF, with and without MPP lining, at the point 23 along the lower y-line

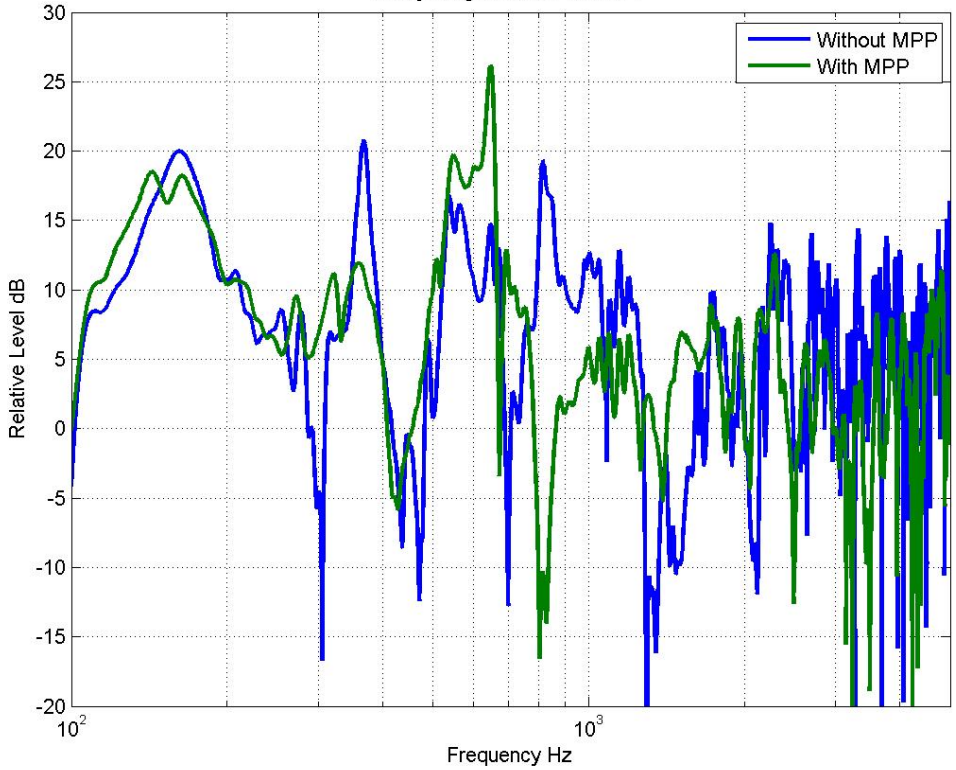

Figure 41. FRF, with and without MPP lining, at the point 24 along the upper y-line

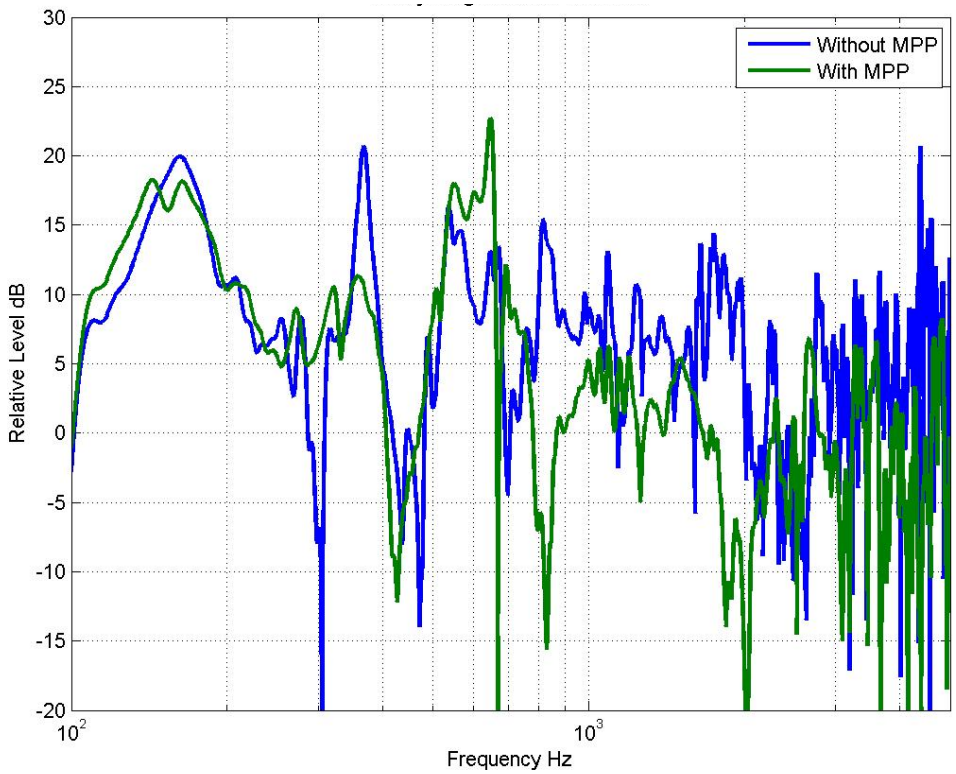

Figure 42. FRF, with and without MPP lining, at the point 25 along the upper y-line

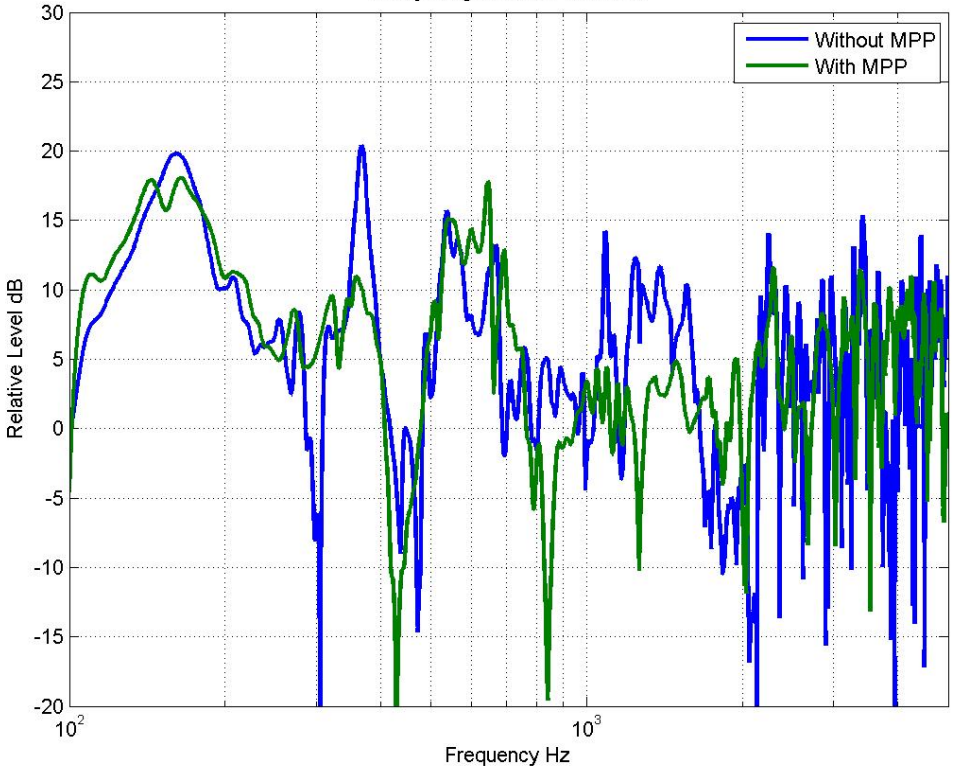

Figure 43. FRF, with and without MPP lining, at the point 26 along the upper y-line

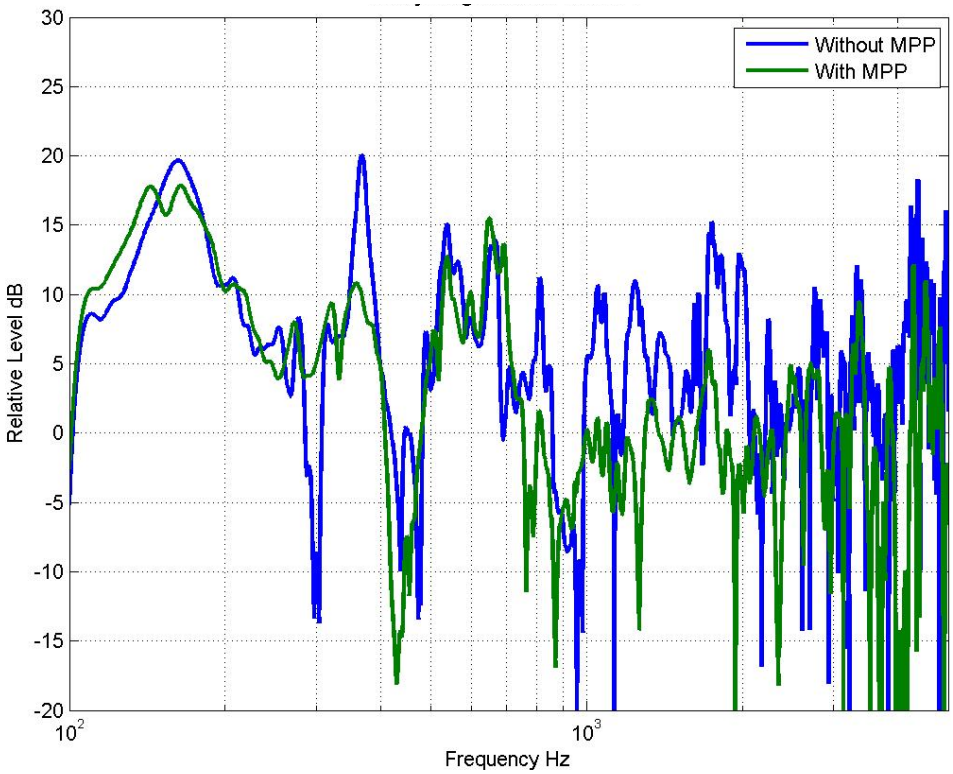

Figure 44. FRF, with and without MPP lining, at the point 27 along the upper y-line

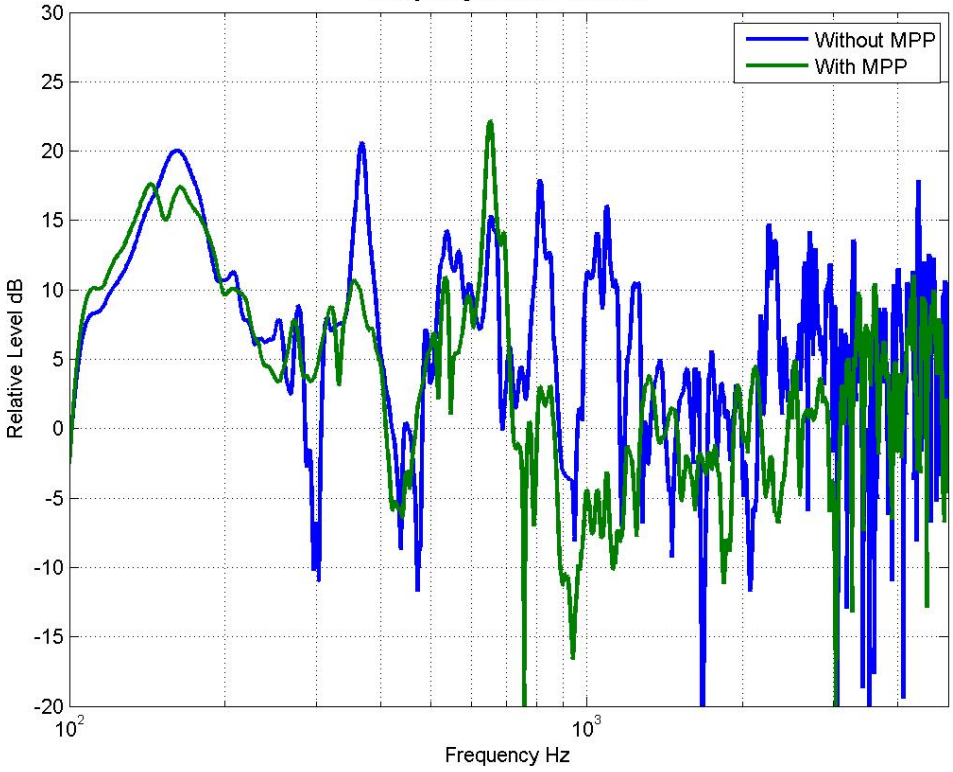

Figure 45. FRF, with and without MPP lining, at the point 28 along the upper y-line

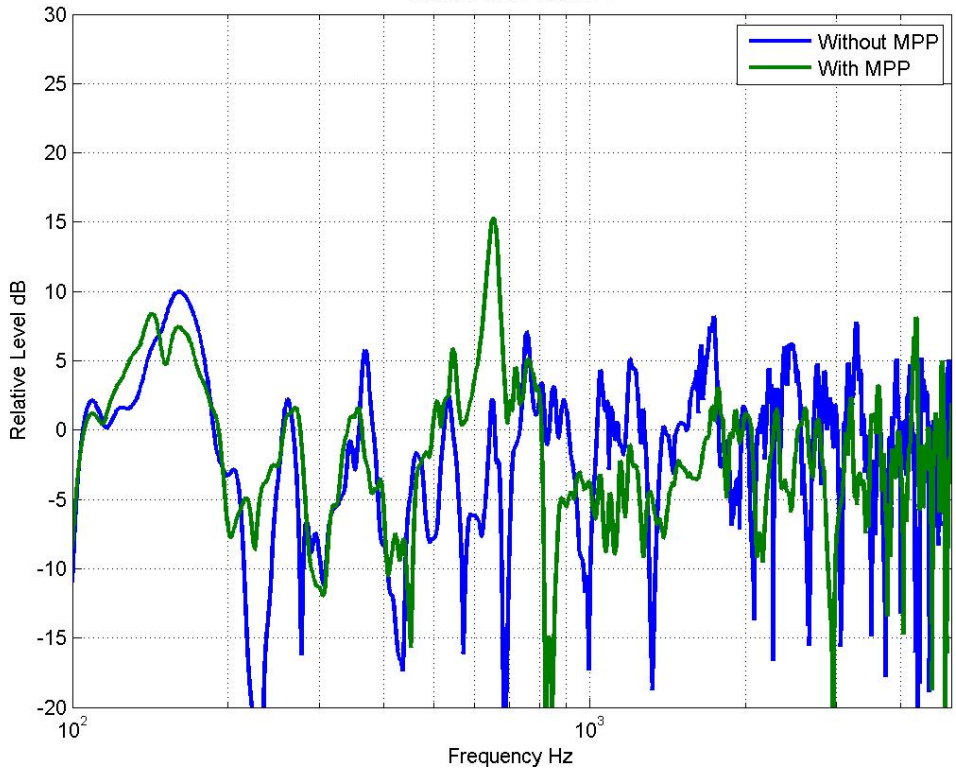

Figure 46. FRF, with and without MPP lining, at the point 29 along the outer x-line

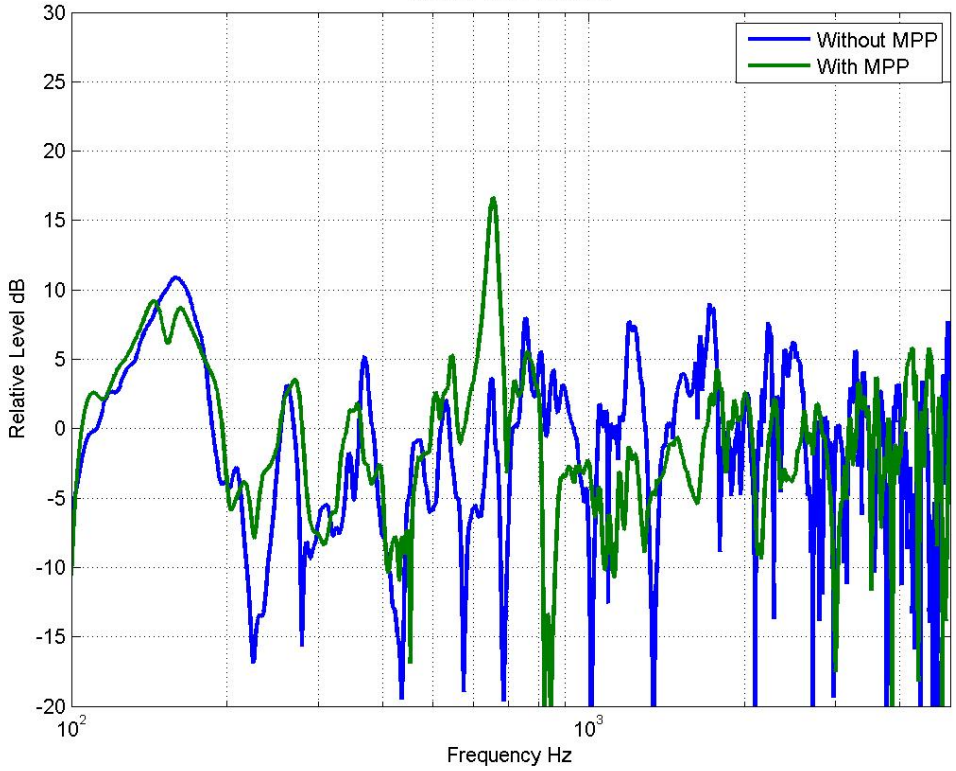

Figure 47. FRF, with and without MPP lining, at the point 30 along the outer x-line

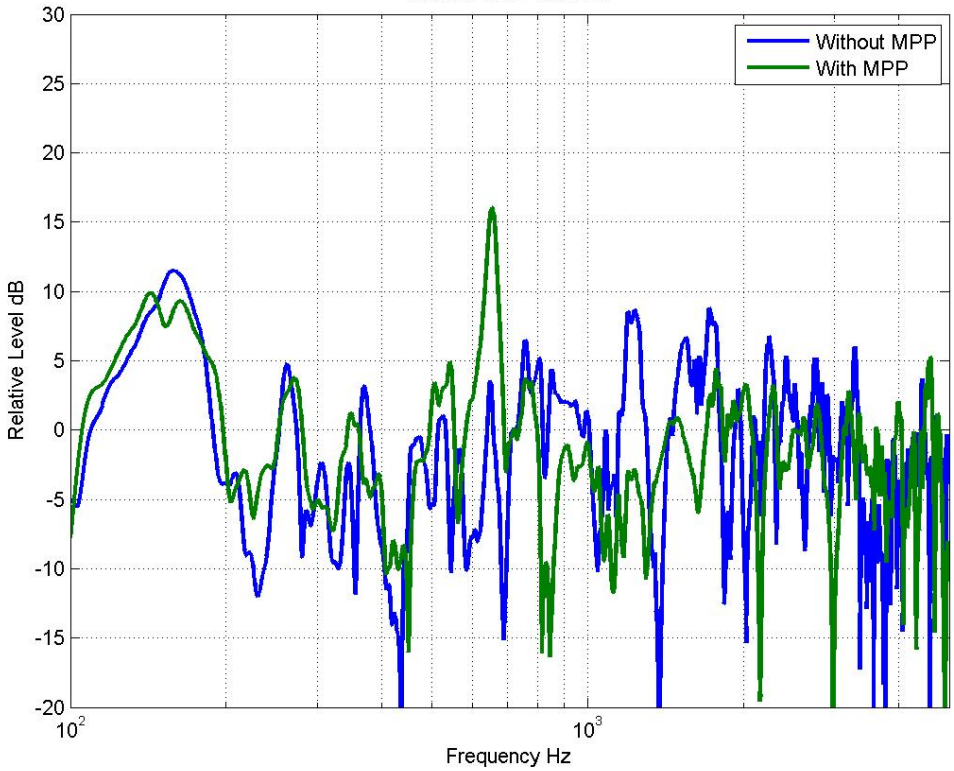

Figure 48. FRF, with and without MPP lining, at the point 31 along the outer x-line

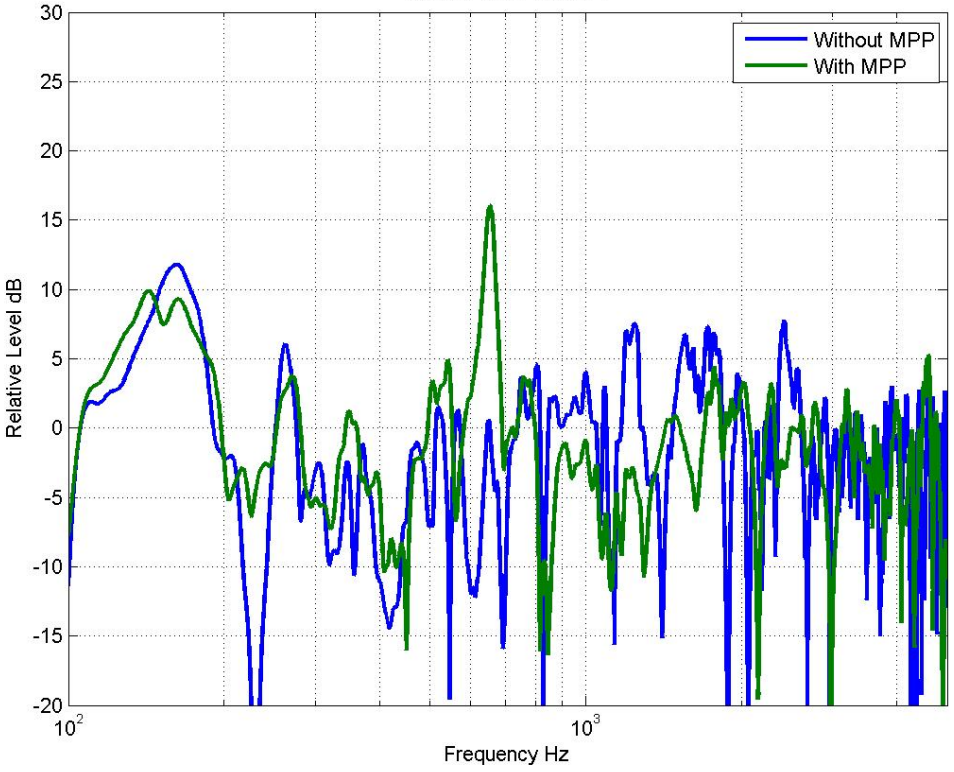

Figure 49. FRF, with and without MPP lining, at the point 32 along the outer x-line

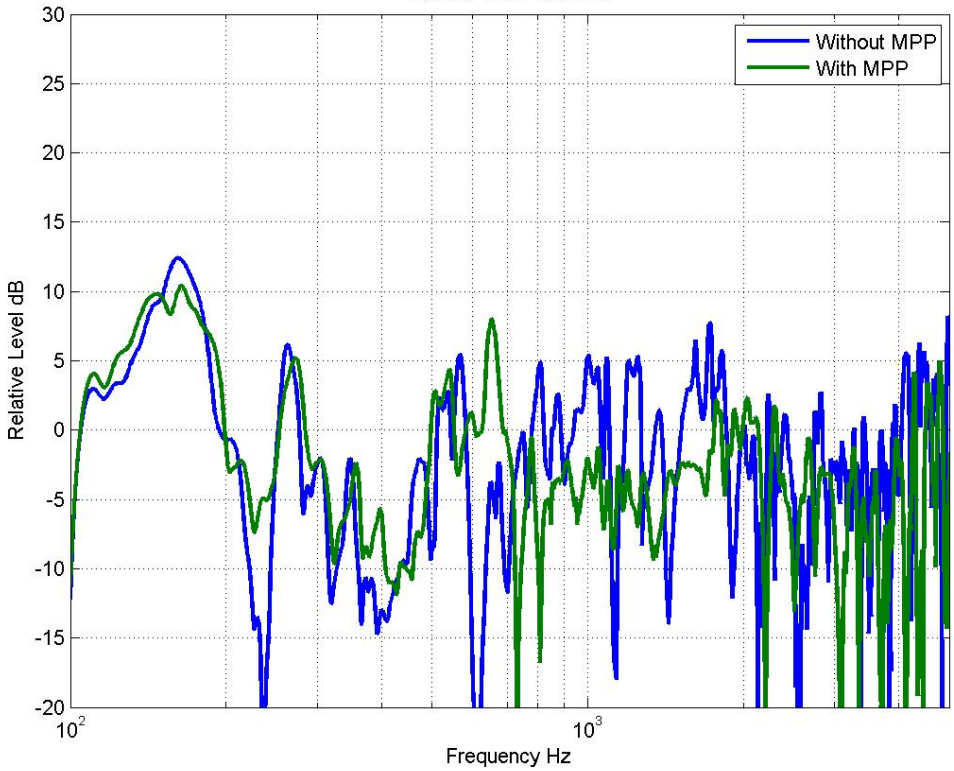

Figure 50. FRF, with and without MPP lining, at the point 33 along the outer x-line

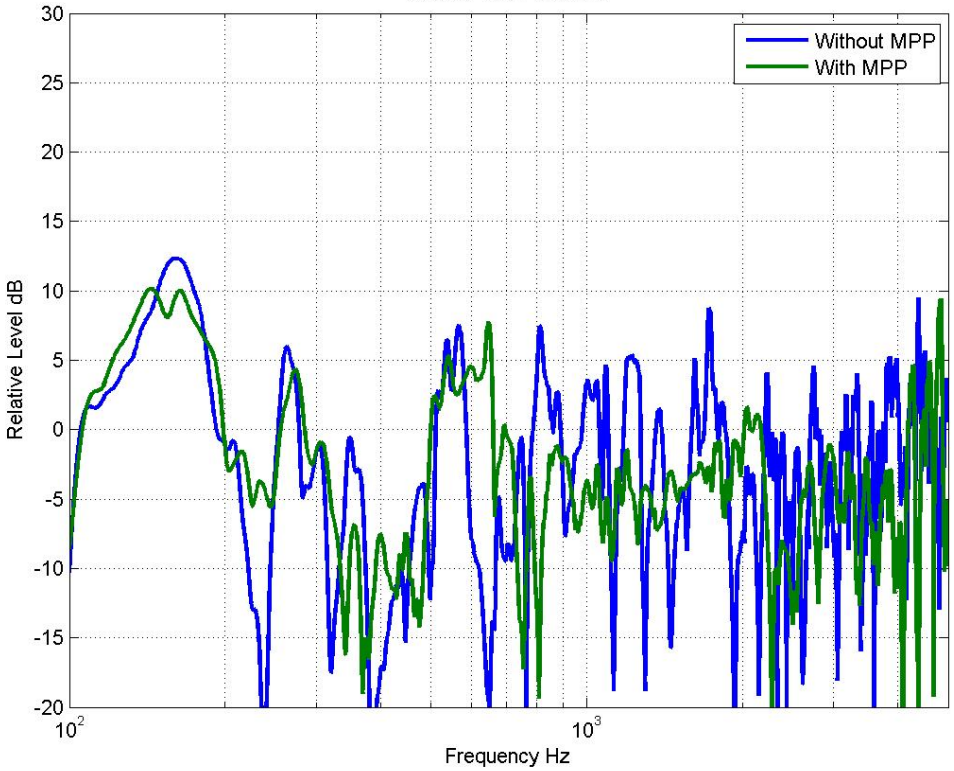

Figure 51. FRF, with and without MPP lining, at the point 34 along the outer x-line

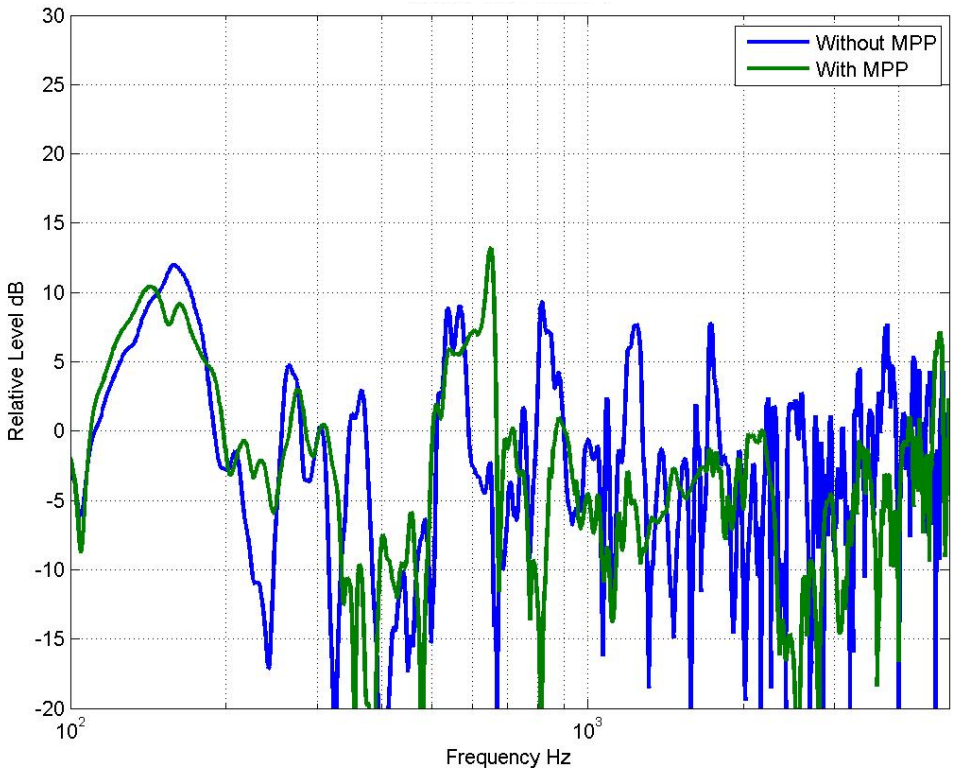

Figure 52. FRF, with and without MPP lining, at the point 35 along the outer x-line

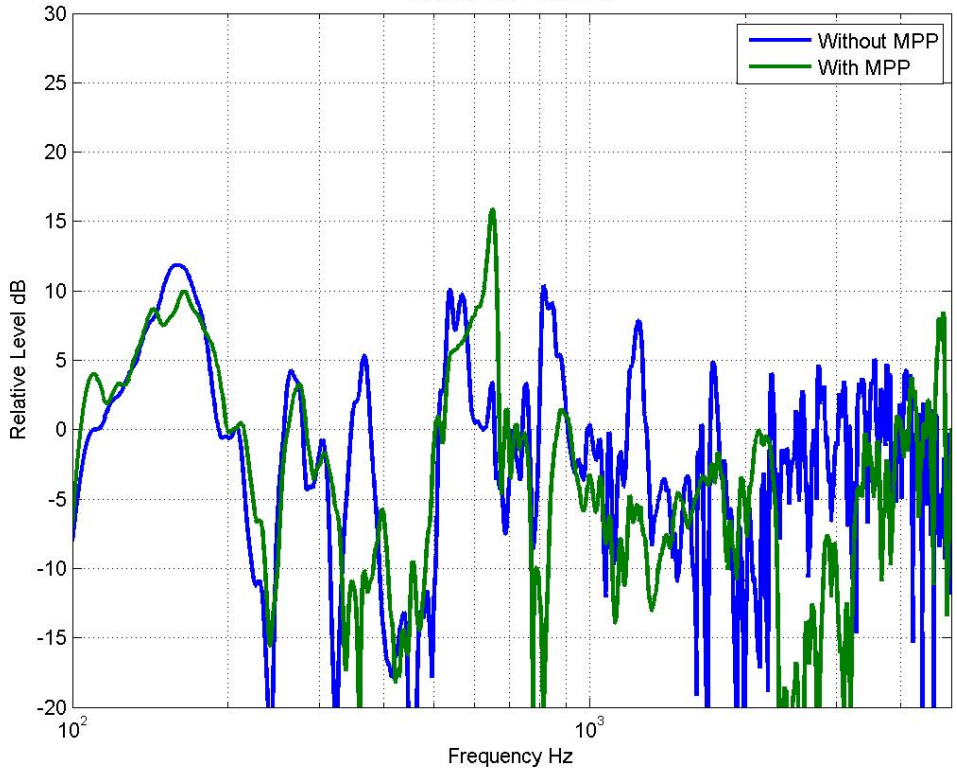

Figure 53. FRF, with and without MPP lining, at the point 36 along the outer x-line

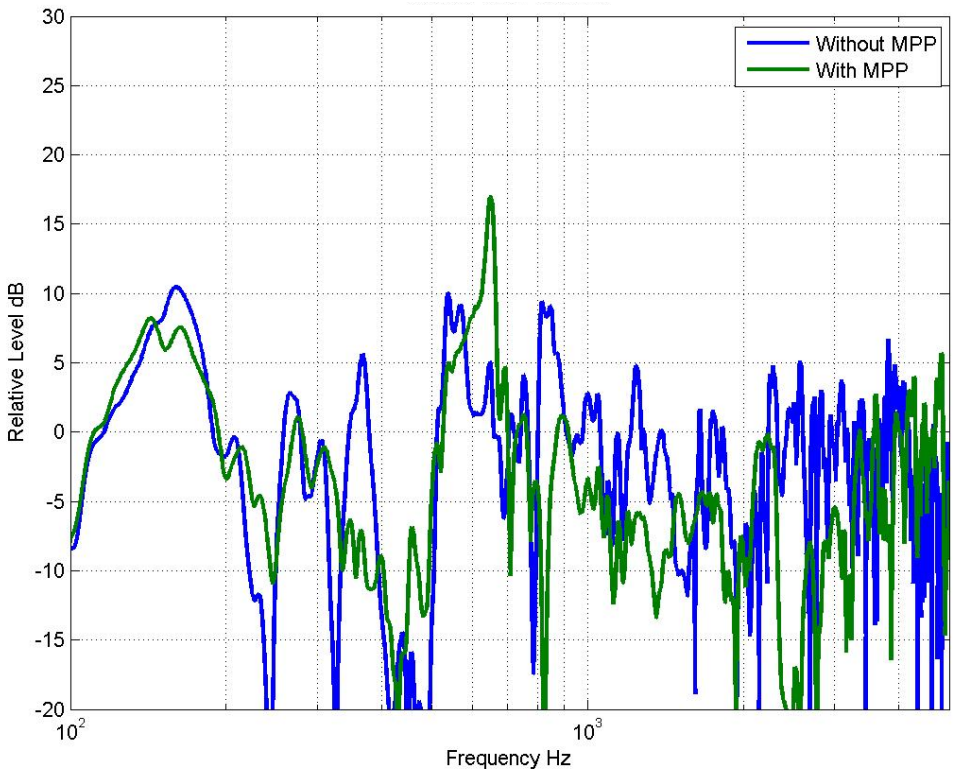

Figure 54. FRF, with and without MPP lining, at the point 37 along the outer x-line

Perhaps, the sound level reduction due to the liner absorption could be better appreciated if the x-axis of the FRFs were depicted in proportional bands. Figures 55-59 show the attenuation of the FRF magnitude due to the MPP liner at the inner x and y-lines (lower and upper) and the outside line, at 1/3 octave bands between 800 and 3150 Hz. Here, the attenuation is calculated as the energetic difference of FRF magnitudes, without and with the MPP lining, at the proportional bands centred at the 1/3 central frequencies. Negative attenuations at some bands are due to the sound reinforcement. As it can be seen, MPP lining produces attenuation at most of the measurement points and most of the 1/3 octave frequency bands, with some noticeable exceptions. For example, reinforcement is produced at most points in the lower x-line at 1600 Hz, in the upper x-line at 2000 Hz, and in the outer x-line also at 2000 Hz.

It can be illustrative to show the average attenuation along the lower and upper x and y lines, and along the outer x-lines. These average attenuations are shown in Figures 60-64.

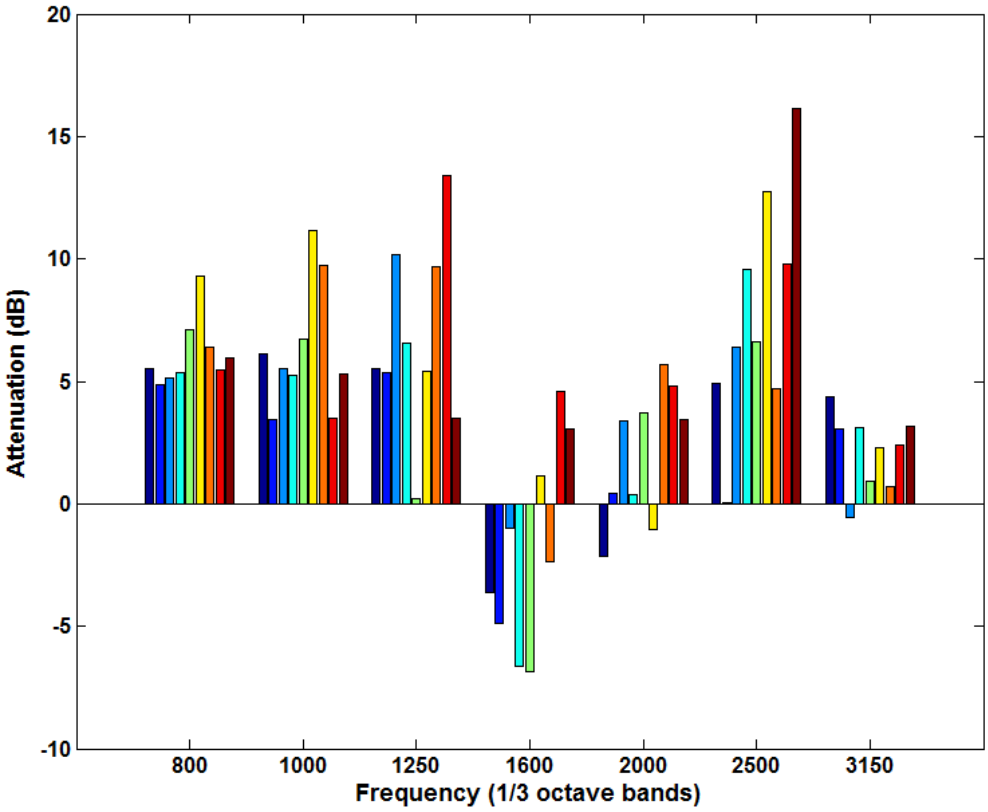

Figure 55. Attenuation of the FRF magnitude at points of the lower x-line due to MPP lining

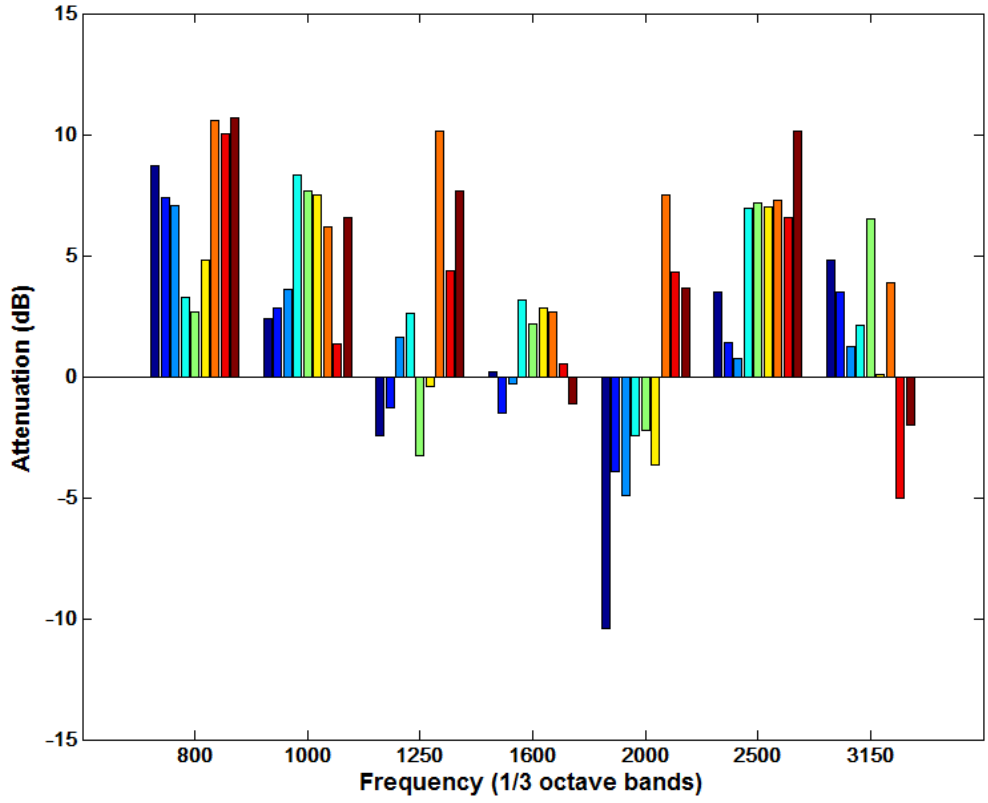

Figure 56. Attenuation of the FRF magnitude at points of the upper x-line due to MPP lining

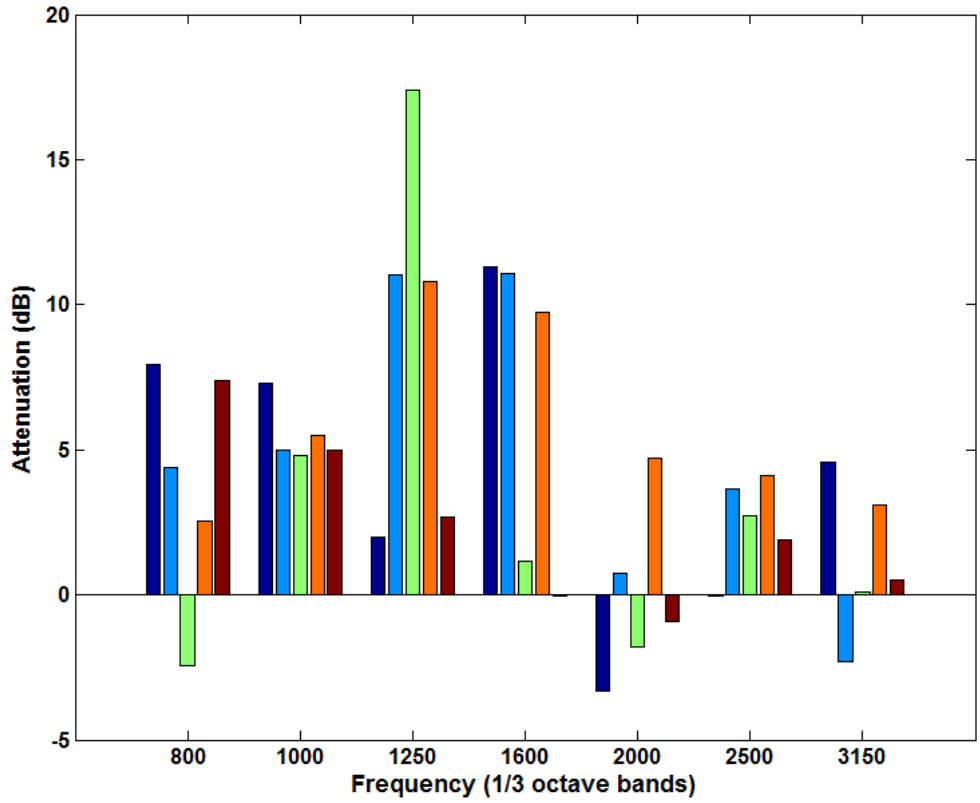

Figure 57. Attenuation of the FRF magnitude at points of the lower y-line due to MPP lining

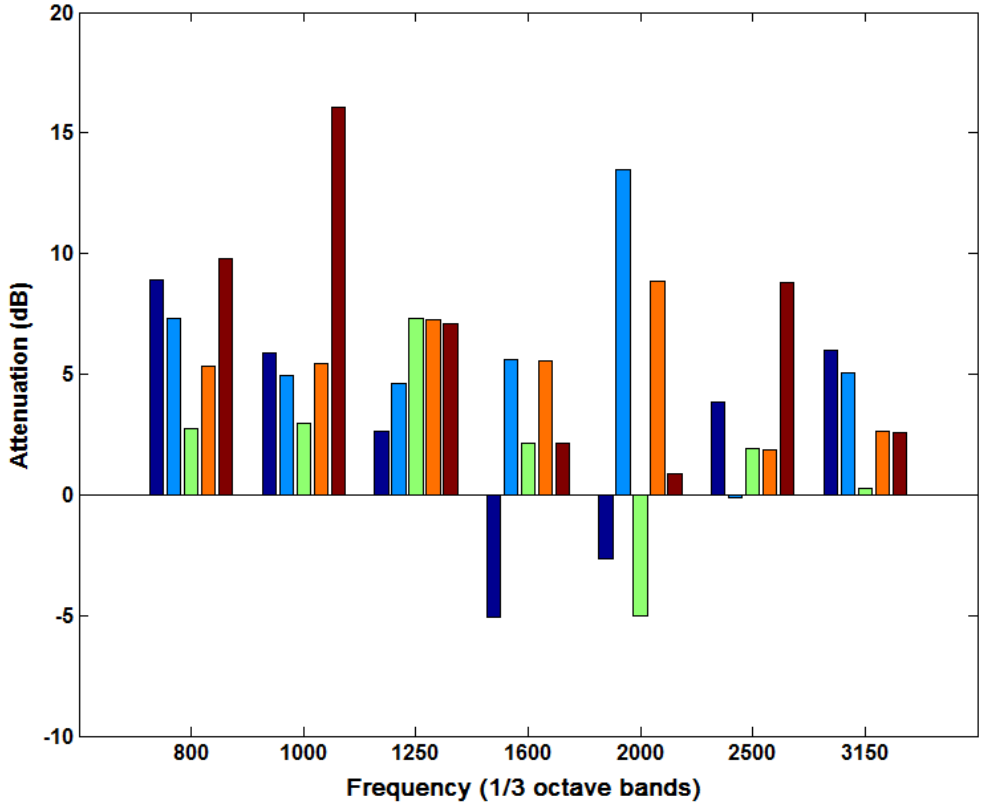

Figure 58. Attenuation of the FRF magnitude at points of the upper y-line due to MPP lining

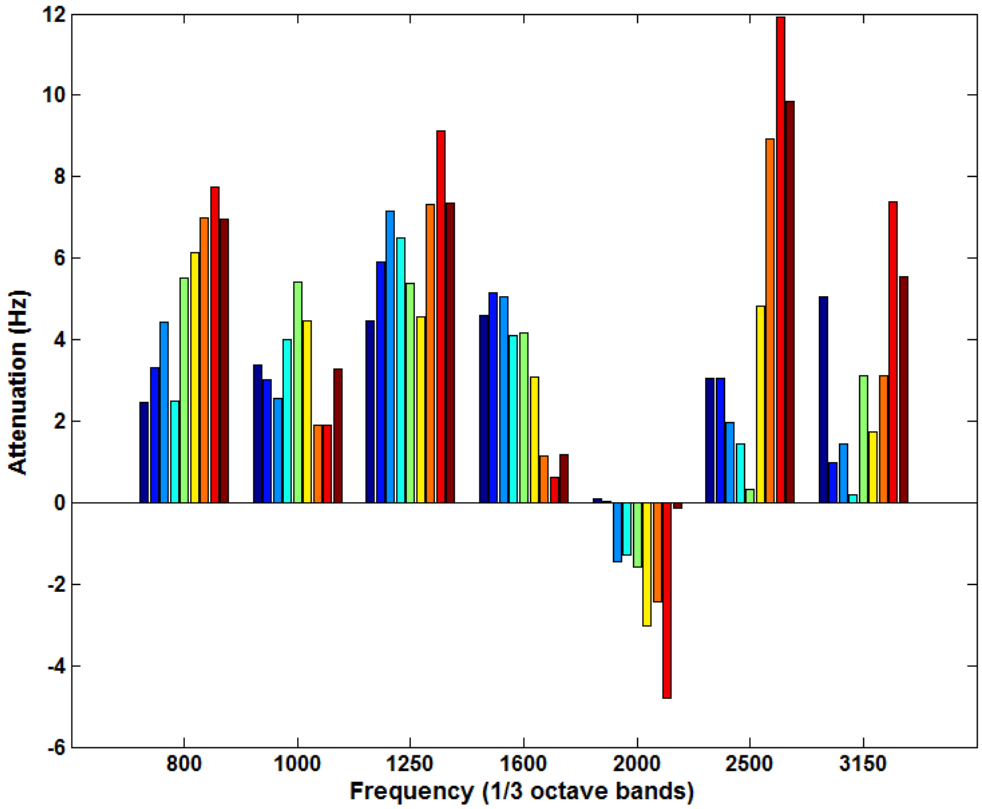

Figure 59. Attenuation of the FRF magnitude at points of the outside x-line due to MPP lining

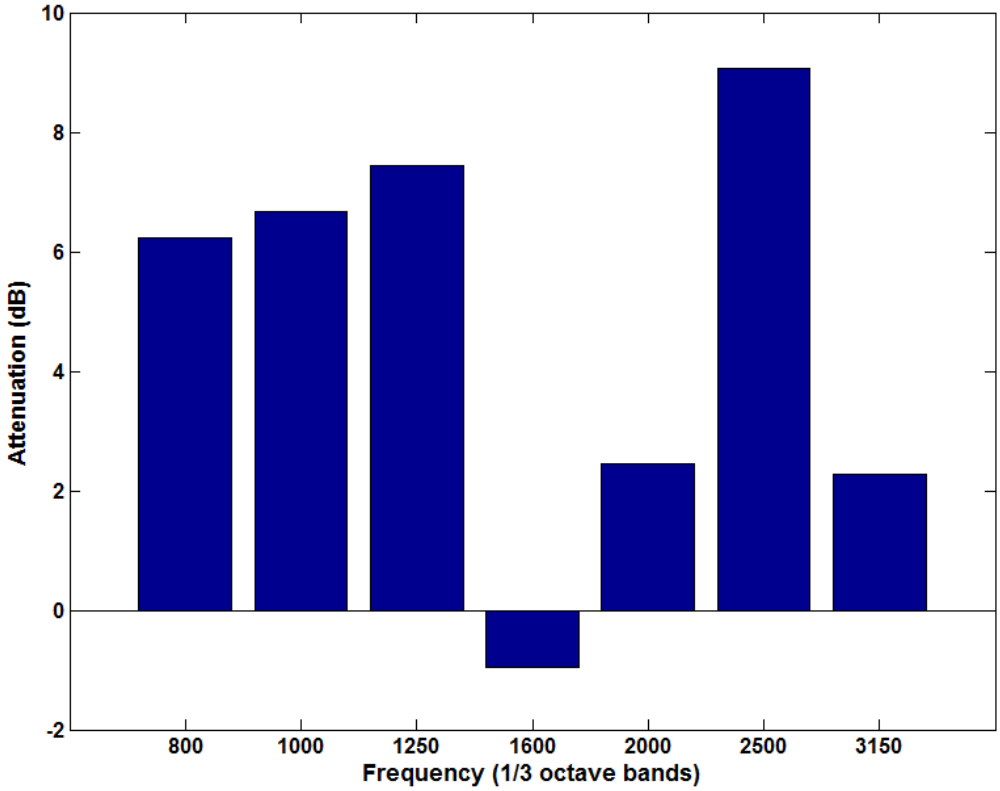

Figure 60. Average attenuation due to MPP lining along the lower x-line

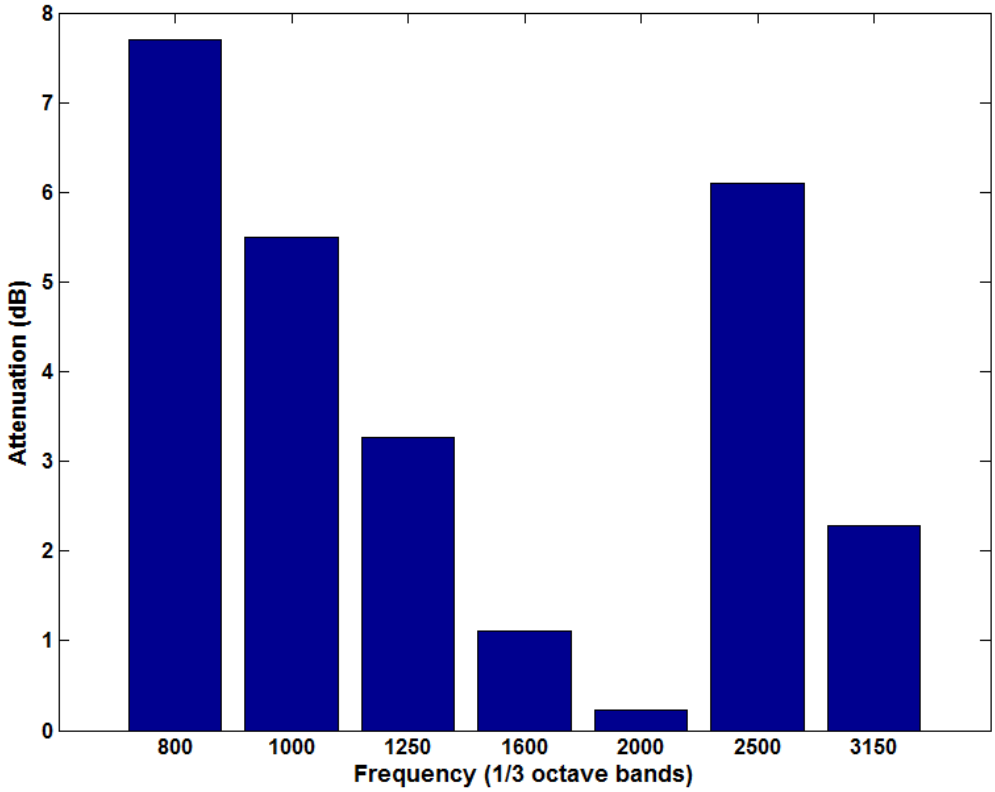

Figure 61. Average attenuation due to MPP lining along the upper x-line

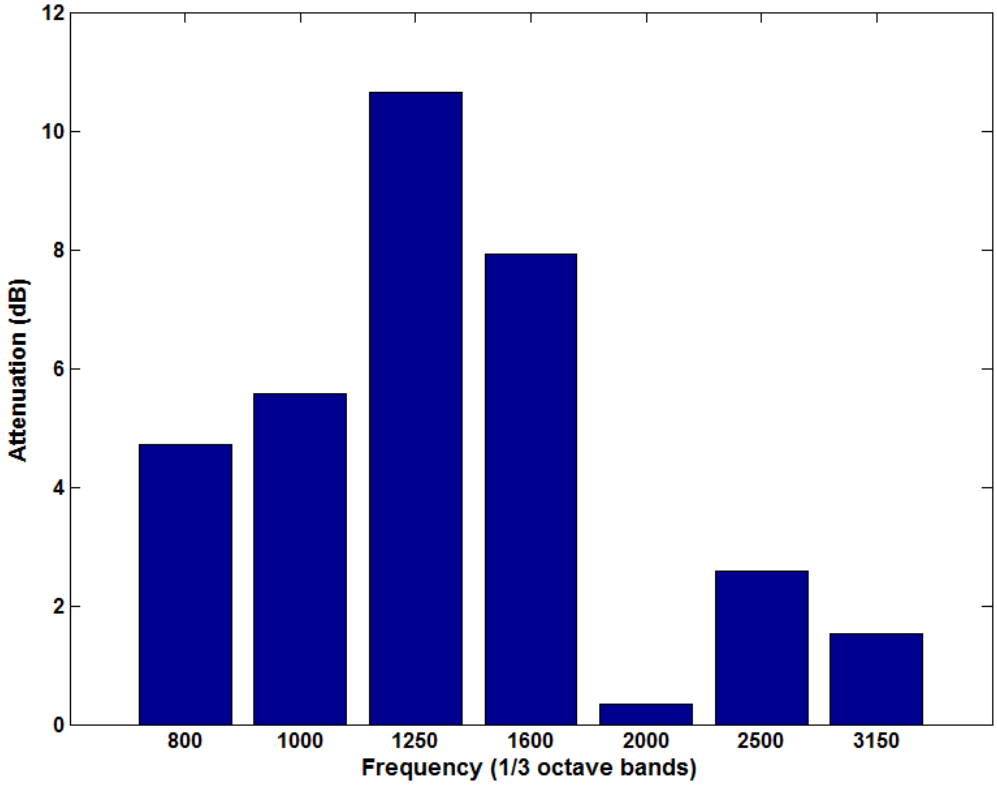

Figure 62. Average attenuation due to MPP lining along the lower y-line

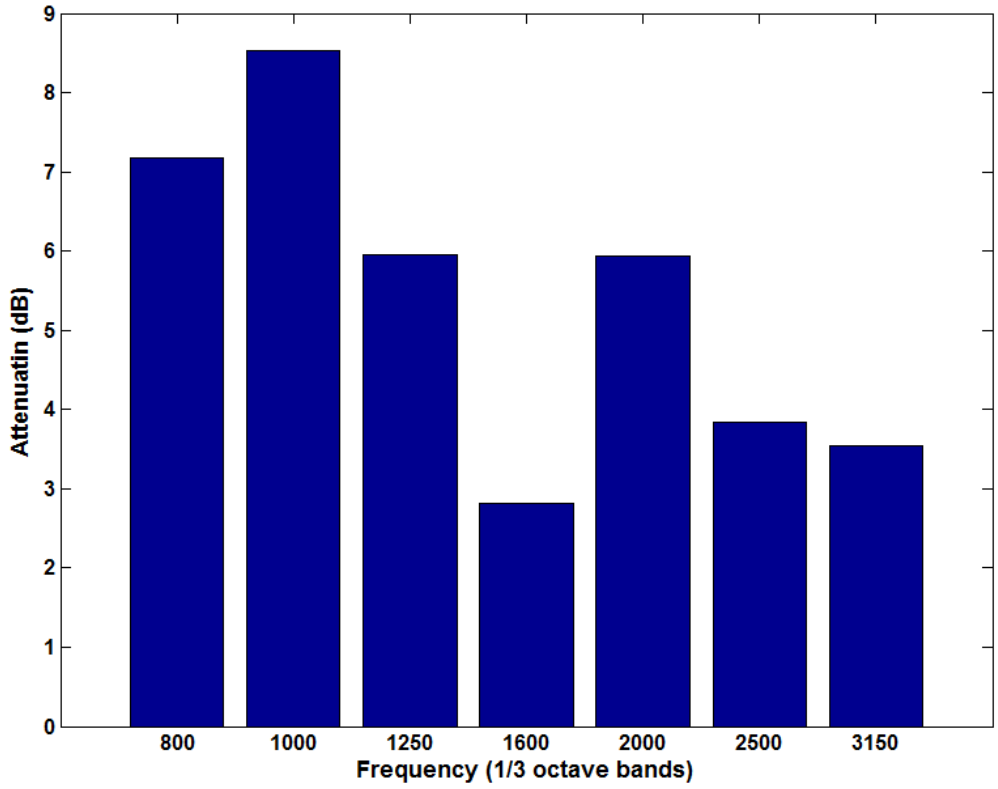

Figure 63. Average attenuation due to MPP lining along the upper y-line

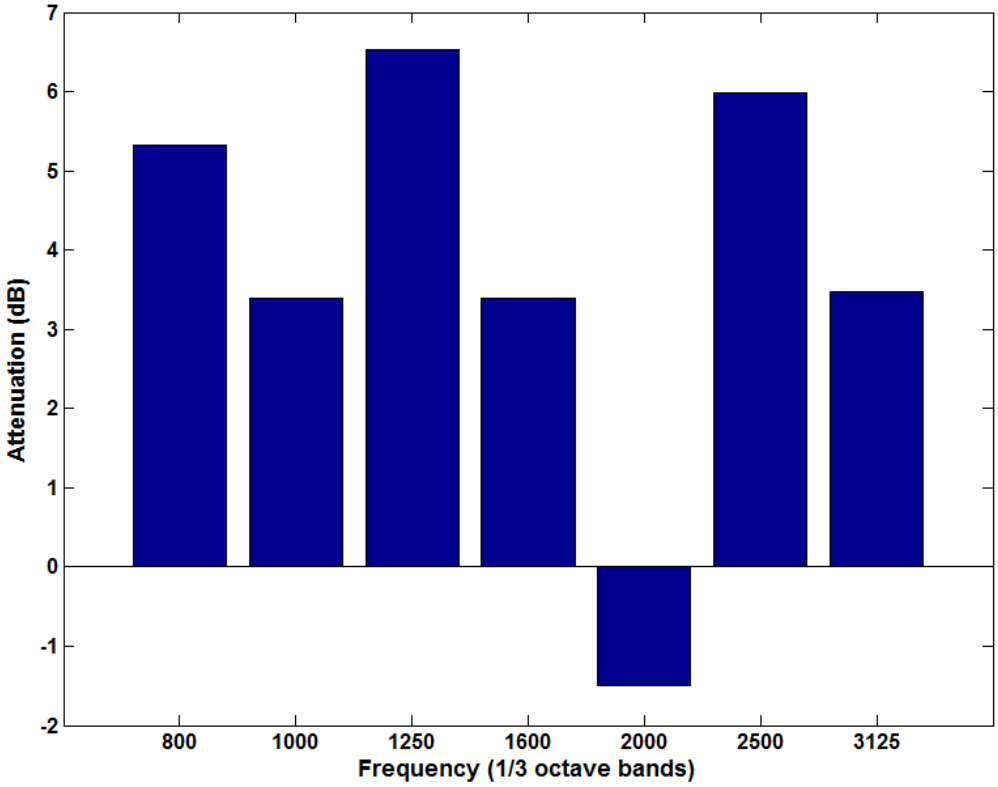

Figure 64. Average attenuation due to MPP lining along the outer x-line

7. SUMMARY AND CONCLUSIONS

The effect of lining the inner wall of an open cavity in the acoustic field inside and outside the cavity has been experimentally analysed. We have used a wooden open cavity constructed previously, changing the former 4” loudspeaker for an inverse filtered point source. Also, the inner walls of the cavity have been lined with MPPs manufactured by an infiltration technique. The MPPs have been designed to provide absorption in a frequency band ranging from 800 to 2000 Hz.

The resonance frequencies of the cavity have been elucidated experimentally measuring the impulse responses between a fixed source and a microphone moving along points inside and outside the cavity. The Fourier transform of these impulse responses to the frequency domain gives the FRF functions at each measurement point. The peaks of the FRFs are then identified as the resonance frequencies of the open cavity.

The effect of lining the inner walls with MPPs is to attenuate the resonance peaks in the frequency band were the MPPs were designed to absorb sound. At lower frequencies, however, some of the resonance peaks of the cavity are deleteriously reinforced.

ACKNOWLEDGEMENTS

One of the authors (Cristobal González) has been financed by the European Union through Grant PIEF-GA- 2011-301287.

REFERENCES

Atalla, N., Sgard, J.F., 2007. “Modeling of perforated plates and screens using rigid frame porous models.” J. Sound Vib., 303: 195-208.

Chevillotte, F., 2012. “Controlling sound absorption by an upstream resistive layer.” App. Acoust., 73, 56-60.

Cobo, P., Fernández, A., Cuesta, M., 2007. “Measuring short impulse responses with inverse filtered máximum-length sequences.” Appl. Acoust., 68, 820-830.

Cobo, P., Ruiz, H., Alvarez, J., 2010. “Double-layer microperforated panel/porous absorber as liner for anechoic closing of the test section in wind tunnels.” Acta Acustica united with Acustica, 96, 914-922.

Cobo, P., Ortiz, S., Ibarra, D., De la Colina, C., 2013. “Point source equalised by inverse filtering for measuring ground impedance.” Appl. Acoust., 74, 561-565.

Cobo, P., Montero de Espinosa, F., 2013. “Proposal of cheap microperforated panel absorbers manufactured by infiltration.” Appl. Acoust., 74, 1069-1075.

Maa, D.Y., 1987. “Microperforated-panel wideband absorbers.” Noise Control Eng. J., 29, 77-84.

Maa, D.Y., 1998. “Potential of microperforated panel absorber.” J. Acoust. Soc. Am., 104, 2861-2866.

Ortiz, S., Le Plenier, C., Cobo, P., 2013. “Efficient modelling and experimental validation of acoustic resonances in thre-dimensional rectangular open cavities.” Appl. Acoust., 74, 949-957.

Ortiz, S., Kolbrek, B., Cobo, P., González, L., de la Colina, C., 2014. “Point source loudspeaker design: Advances on the inverse horn approach.” Sent to J. Audio Eng. Soc.

Polak, J.D., Chistensen L.S., Juhl, P.M., 2001. “An innovative design for omnidirectional sound sources.” Acta Acustica uw ACUSTICA, 87, 505-512.